Atmos. Chem. Phys. Discuss., 15, 17397–17448, 2015
www.atmos-chem-phys-discuss.net/15/17397/2015/
doi:10.5194/acpd-15-17397-2015

Atmospheric Chemistry and Physics Discussions

A process-based ^{222}Rn flux map for Europe and its comparison to long-term observations

U. Karstens[1], **C. Schwingshackl**[2,*], **D. Schmithüsen**[2], **and I. Levin**[2]

[1]Max-Planck-Institut für Biogeochemie, Jena, Germany
[2]Institut für Umweltphysik, Heidelberg University, Heidelberg, Germany
[*]now at: Institute for Atmospheric and Climate Science, ETH Zürich, Switzerland

Received: 21 May 2015 – Accepted: 09 June 2015 – Published: 25 June 2015

Correspondence to: U. Karstens (ukarst@bgc-jena.mpg.de)

Published by Copernicus Publications on behalf of the European Geosciences Union.

Abstract

Detailed ^{222}Rn flux maps are an essential prerequisite for the use of radon in atmospheric transport studies. Here we present a high-resolution ^{222}Rn flux map for Europe, based on a parameterization of ^{222}Rn production and transport in the soil. The ^{222}Rn exhalation rate was parameterized based on soil properties, uranium content, and modelled soil moisture from two different land-surface reanalysis data sets. Spatial variations in exhalation rates are primarily determined by the uranium content of the soil, but also influenced by local water table depth and soil texture. Temporal variations are related to soil moisture variations as the molecular diffusion in the unsaturated soil zone depends on available air-filled pore space. The implemented diffusion parameterization was tested against campaign-based ^{222}Rn profile measurements. Monthly ^{222}Rn exhalation rates from European soils were calculated with a nominal spatial resolution of $0.083^{\circ} \times 0.083^{\circ}$ and compared to long-term direct measurements of ^{222}Rn exhalation rates in different areas of Europe. The two realizations of the ^{222}Rn flux map, based on the different soil moisture data sets, both realistically reproduce the observed seasonality in the fluxes but yield considerable differences for absolute flux values. The average ^{222}Rn flux from soils in Europe is estimated to be 10 or 15 mBq m^{-2} s^{-1}, depending on the soil moisture data set, and the seasonal variations in the two realisations range from 7.1 mBq m^{-2} s^{-1} in February to 13.9 mBq m^{-2} s^{-1} in August and from 10.8 mBq m^{-2} s^{-1} in March to 19.7 mBq m^{-2} s^{-1} in July, respectively. This systematic difference highlights the importance of realistic soil moisture data for a reliable estimation of ^{222}Rn exhalation rates.

1 Introduction

One of the limiting factors for applying atmospheric ^{222}Rn measurements for transport model validation is a reliable, high-resolution ^{222}Rn flux map for the global continents, but also on the regional scale for Europe. It has been shown earlier that the assumption

ACPD
15, 17397–17448, 2015

of a constant exhalation rate of 1 atom cm^{-2} s^{-1} for continental areas, as was proposed by Jacob and Prather (1990) as an intermediate value from data reported by Wilkening et al. (1972) and Turekian et al. (1977), is an over-simplification of the true conditions, in particular for Europe (Dörr and Münnich, 1990; Schüßler, 1996; Conen and Robertson, 2002). Nevertheless, this assumption was used, for simplicity, in different transport model estimates and model inter-comparison studies (Rasch et al., 2000; Chevillard et al., 2002; Taguchi et al., 2011). Only in the last decade, a number of attempts have been made to develop high-resolution maps of the variability of ^{222}Rn exhalation from continental soils (Schery and Wasiolek, 1998; Sun et al., 2004; Zhuo et al., 2008; Szegvary et al., 2009; Griffith et al., 2010; Hirao et al., 2010; López-Coto et al., 2013). We present here a high-resolution ^{222}Rn flux map for Europe, based on a parameterization of ^{222}Rn production and transport in the soil.

^{222}Rn is a progeny of ^{238}U, a trace element in natural soils. Since ^{222}Rn is the first gaseous element in the ^{238}U decay chain, all daughter nuclides from ^{238}U up to ^{226}Ra, the mother nuclide of ^{222}Rn, are often assumed to be in equilibrium in the soil. Besides the ^{226}Ra content, ^{222}Rn exhalation rates also strongly depend on soil properties. Therefore, not only the ^{238}U content but also the parameters influencing diffusive transport characteristics of the soil need to be known to properly estimate the variability of ^{222}Rn exhalation rates (Schüßler, 1996). Taking these into account, Griffith et al. (2010) developed a high-resolution ^{222}Rn flux map for Australian land surfaces. They used a transport model for the unsaturated upper soil layers, national γ-ray surveys, maps of soil properties, such as porosity and bulk density, as well as modelled soil moisture to estimate monthly ^{222}Rn exhalation rates at 0.05° spatial resolution. Likewise, López-Coto et al. (2013) published a ^{222}Rn flux map for Europe that also uses numerical modelling of ^{222}Rn transport in the upper soil layers. Their input parameters were measured ^{238}U activity concentrations from the Geochemical Atlas of Europe (Salminen, 2005) and other soil properties as well as modelled soil temperature and moisture data. Based on these parameters, they estimated average monthly ^{222}Rn exhalation rates for the time period of 1957–2002 at a spatial resolution of 1 km.

ACPD
15, 17397–17448, 2015

Szegvary et al. (2007b) found an empirical relation between ^{222}Rn exhalation rate and γ-dose rate. Following this finding, Szegvary et al. (2009) published a ^{222}Rn flux map for Europe that solely uses γ-dose rate as a proxy for ^{222}Rn exhalation rate.

In the present work, we use a similar approach as Griffith et al. (2010) for Australia and López-Coto et al. (2013) for Europe. We estimate the ^{222}Rn exhalation rate from European land surface based on the measured distribution of ^{238}U in the upper soil layers (Salminen, 2005), the soil texture class distribution (Reynolds et al., 2000) as well as model estimates of the soil moisture, which largely governs molecular diffusion in the unsaturated soil. For the period of 2006 to 2010, we test two different soil moisture reanalysis data sets, i.e. (1) from the Noah Land Surface Model in the Global Land Data Assimilation System (GLDAS-Noah, Rodell et al., 2004), and (2) from the ERA-Interim/Land reanalysis (Balsamo et al., 2015). Soil moisture-dependent molecular diffusive transport in the upper meter of the soil is calculated based on the Millington and Quirk (1960) model. The validity of our diffusion model approach is tested at different soil moisture regimes, using systematic ^{222}Rn soil profile measurements at our observational site close to Heidelberg, Germany. The European flux maps are further compared to direct spot and long-term measurements of ^{222}Rn exhalation rates in different areas across Europe.

2 Theoretical considerations

2.1 Basic equations for ^{222}Rn production, decay and diffusion in soils

The derivations below essentially follow those presented in Dörr and Münnich (1990), Born et al. (1990), Schüßler (1996), and Griffiths et al. (2010). They are valid for an infinitely deep unsaturated homogeneous soil and we consider only changes of concentration $c(z,t)$, flux $j(z,t)$ as well as source $Q(z,t)$ or sink strength $S(z,t)$ in the vertical direction z (with the z coordinate defined as positive downwards and $z = 0$ at the soil–atmosphere interface).

ACPD
15, 17397–17448, 2015

In this case the equation of continuity in the soil air can be reduced to one spatial dimension, namely

$$\frac{\mathrm{d}c(z,t)}{\mathrm{d}t} + \frac{\partial j(z,t)}{\partial z} = Q(z,t) + S(z,t). \quad (1)$$

We further assume that, at any depth in the soil, the only sink process is radioactive decay, which is described by

$$S(z,t) = -\lambda c(z,t) \quad (2)$$

with the decay constant $\lambda(^{222}\mathrm{Rn}) = 2.0974 \times 10^{-6}\,\mathrm{s}^{-1}$.

The source term Q, i.e. the production rate of ^{222}Rn gas in the soil, is calculated according to Schüßler (1996) from

$$Q(z) = \lambda \rho_\mathrm{b}(z) c_\mathrm{Ra}(z) \varepsilon(z) \quad (3)$$

with ρ_b the dry bulk density of the soil ($\mathrm{kg\,m^{-3}}$), c_Ra the ^{226}Ra activity concentration in the soil material ($\mathrm{Bq\,kg^{-1}}$), and ε the ^{222}Rn emanation coefficient, which is defined as the probability that a ^{222}Rn atom produced in a soil grain can actually escape into the soil air.

If we consider steady state conditions, i.e. no explicit dependence on time, Eq. (1) simplifies to

$$0 = -\frac{\partial j(z)}{\partial z} + Q(z) + S(z) = -\frac{\partial j(z)}{\partial z} + Q(z) - \lambda c(z) \text{ or}$$

$$\frac{\partial j(z)}{\partial z} = Q(z) - \lambda c(z). \quad (4)$$

Taking into account only molecular diffusion of the trace gas in the soil air with P, the permeability of the soil, assumed here to be constant with depth, we can apply Fick's first law

$$j(z) = -P \frac{\partial c(z)}{\partial z}. \quad (5)$$

ACPD
15, 17397–17448, 2015

Note that in Eq. (5) $j(z)$ is the flux per unit area of the bulk soil. This is not immediately obvious and in the respective Eq. (1) in Griffith et al. (2010), and also in Sun et al. (2004) $j(z)$ is multiplied with θ_p, the porosity of the soil to yield the flux density per bulk unit area. However, they also use a different expression to calculate the source strength Q in the soil (Eq. 3 in Griffith et al., 2010) where they divide our Eq. (3) by θ_p.

Combining Eqs. (4) and (5) yields

$$\frac{\partial^2 c(z)}{\partial z^2} - \frac{\lambda}{P} c(z) = -\frac{Q(z)}{P}. \tag{6}$$

If we further assume that the ^{226}Ra activity concentration in the soil particles, the ^{222}Rn emanation coefficient, and the soil bulk density are constant with depth, we obtain a depth-independent source strength, i.e. $Q(z) = Q$, and Eq. (6) becomes

$$P\frac{\partial^2 c(z)}{\partial z^2} - \lambda c(z) + Q = 0. \tag{6a}$$

2.2 The ^{222}Rn soil air profile and its exhalation rate at the soil surface

The general solution of the inhomogeneous differential Eq. (6a) is

$$c(z) = c_\infty(1 - e^{-\frac{z}{\bar{z}}}),$$

where c_∞ is the asymptotic concentration at large depths and $\bar{z}$ the relaxation depth.

With the boundary conditions that (1) at the soil–air interface the ^{222}Rn activity concentration approaches zero and (2) at large depths there is no change of the concentration with depth, i.e. equilibrium between ^{222}Rn production and decay,

$$c(z = 0) = 0 \text{ and } \frac{\mathrm{d}c}{\mathrm{d}z}(z = \infty) = 0,$$

ACPD
15, 17397–17448, 2015

the solution of Eq. (6a) gets

$$c(z) = c_\infty(1 - e^{-\frac{z}{\bar{z}}}) = \frac{Q}{\lambda}\left(1 - e^{-\sqrt{\frac{\lambda}{P}}z}\right) \tag{7}$$

$$\text{i.e. } c_\infty = \frac{Q}{\lambda} \text{ and } \bar{z} = \sqrt{\frac{P}{\lambda}}. \tag{7a}$$

Introducing solution Eq. (7) into the diffusion Eq. (5) we can calculate the ^{222}Rn flux at the soil surface

$$j(z=0) = -P\frac{\partial c(z)}{\partial z}\bigg|_{z=0} = -P\frac{c_\infty}{\bar{z}} = -\bar{z}c_\infty\lambda = -Q\sqrt{\frac{P}{\lambda}} = -\rho_b c_{Ra}\varepsilon\sqrt{P\lambda}. \tag{8}$$

Note that the last term in Eq. (8), which allows calculating the ^{222}Rn flux density per unit bulk surface of the soil from "bottom-up" parameters and the permeability in the soil, is now identical to Eq. (4) in Griffith et al. (2010).

2.3 Approximation of ^{222}Rn fluxes at sites with shallow water table depth

The solution of the differential Eq. (6a) given by Eqs. (7) and (7a) is only valid if we can assume an infinitely deep unsaturated soil. This assumption is not always fulfilled. Particularly in Northern Europe or in Siberian wetland areas the water table depth can be as close to the surface as 10 or 20 cm. In that case there is only a very shallow soil depth available for ^{222}Rn production and exhalation into the atmosphere (if we consider that the molecular diffusion coefficient of ^{222}Rn in water is lower by 2–3 orders of magnitude compared to air, and that there is only negligible ^{222}Rn flux from ground water into the unsaturated soil zone). In order to estimate ^{222}Rn exhalation rates in such situations, we can make a first order budget approach. Assuming the water table depth at $z = z_G$ we can balance the ^{222}Rn inventory (i.e. the standing crop) in the unsaturated

ACPD
15, 17397–17448, 2015

part of the soil as follows:

$$c_\infty z_G = \int_0^{z_G} c(z)\mathrm{d}z - \frac{j(z=0)}{\lambda} \text{ or } \frac{j(z=0)}{\lambda} = -c_\infty z_G + \int_0^{z_G} c(z)\mathrm{d}z. \quad (9)$$

Introducing the general solution from Eq. (6) in

$$\int_0^{z_G} c(z)\mathrm{d}z = c_\infty \left(z_G - \left(-\overline{z}e^{-\frac{z_G}{\overline{z}}} + \overline{z}\right)\right)$$

and into Eq. (9) yields

$$\frac{j(z=0)}{\lambda} = -c_\infty z_G + c_\infty z_G - c_\infty(\overline{z} - \overline{z}e^{-\frac{z_G}{\overline{z}}}).$$

Then, taking the earlier boundary conditions to estimate c_∞ and $\overline{z}$ according to

$$c_\infty = \frac{Q}{\lambda} \text{ and } \overline{z} = \sqrt{\frac{P}{\lambda}} \quad (7a)$$

gives the modified flux at the surface according to

$$j(z=0) = -Q\sqrt{\frac{P}{\lambda}}(1 - e^{-\frac{z_G}{\overline{z}}}). \quad (8a)$$

The solution Eq. (8a) has the same form as Eq. (8) and for $z_G \gg \overline{z}$ it yields Eq. (8).

Note that the budget Eq. (9) is only an approximation of the real conditions in the unsaturated soil zone in situations when the water table is close to the soil surface because we assume that the concentration profile is the same as if the ground water table was at very large depths. However, it is still a good first approximation of the exhalation flux for areas with a shallow water table depth (Sect. 3.2).

ACPD
15, 17397–17448, 2015

2.4 The role of snow cover and frost on the ^{222}Rn exhalation rate from continental soils

The role of snow cover on the ^{222}Rn exhalation rate is not yet fully understood. Robertson (2004) found in her measurements that a layer of snow had no significant influence on the ^{222}Rn exhalation rate. However, when the top layer of the snow melted and froze again, a smaller ^{222}Rn exhalation rate was measured. This finding suggests that the physical properties of the snow, such as a thin ice layer on its top, determine the magnitude of the ^{222}Rn flux. However, most of the studies cited in Robertson (2004) found no or merely a small effect of snow cover on ^{222}Rn exhalation rate. Thus, although a shielding effect of snow cover has been included in the López-Coto et al. (2013) flux map, this effect is not taken into account in our ^{222}Rn flux estimates.

Another point concerning the ^{222}Rn exhalation rate in winter months is the influence of frozen soils on ^{222}Rn exhalation rates. While different authors e.g. cited by Robertson (2004) report a reduction in ^{222}Rn flux when the soil was frozen, Robertson (2004) found no evidence for a strong influence of frozen soils on ^{222}Rn emissions. However, particularly when soil moisture is high or when an ice layer forms on the ground, this might cause a substantial decrease in ^{222}Rn exhalation rates. Because no systematic analysis of the influence of soil freezing on the ^{222}Rn flux is available our standard ^{222}Rn flux maps do not take into account any positive or negative effect of frozen soil on the exhalation rate. However, we will show one hypothetical scenario of the potential influence of frost on the exhalation rate with reduced fluxes, based on the number of ice days during winter months (Sect. 4.3).

2.5 Estimating the permeability from soil properties

From Eq. (8) we see that the ^{222}Rn flux at the soil surface not only depends on the production rate Q in the soil (see Eq. 3), but also on the permeability P, i.e. on the diffusion coefficient of ^{222}Rn in the soil air. Estimating P in soil air is, however, not a trivial task. This parameter depends mostly on the percentage of soil air volume

ACPD
15, 17397–17448, 2015

available for gas diffusion, but also on the grain size distribution of the soil, i.e. its texture. The unit volume of soil consists of the soil material fraction θ_m, the fraction that is filled with water θ_w, and the air-filled fraction θ_a so that

$$\theta_m + \theta_w + \theta_a = 1 \tag{10}$$

The porosity θ_p of the soil is defined as

$$\theta_p = 1 - \theta_m = \theta_a + \theta_w \tag{10a}$$

Different models were developed in the past to estimate P depending on soil properties and soil moisture. While the more recent models by Moldrup et al. (1996, 1999) require as input detailed parameters of the soil texture, i.e. percentages of clay, coarse sand and fine sand, the earlier models by Millington and Quirk (1960, 1961) and also the parameterization reported by Rogers and Nielson (1991) only require information on soil porosity and soil moisture. The latter parameterization by Rogers and Nielson (1991) has been used by Zhuo et al. (2008), Griffith et al. (2010) and López-Coto et al. (2013) in their ^{222}Rn flux estimates. However, Jin and Jury (1996) could show that the original estimate of the permeability according to Millington and Quirk (1960), i.e.

$$P = D\frac{\theta_a^2}{\theta_p^{\frac{2}{3}}} = D\frac{\left(\theta_p - \theta_w\right)^2}{\theta_p^{\frac{2}{3}}} \tag{11}$$

(where $D = 1.1 \times 10^{-5}\,\mathrm{m^2\,s^{-1}}$ is the diffusion coefficient of radon in air) yields excellent agreement with a large set of available observational data of the permeability P for soils with different texture obtained from different studies in the literature (Jin and Jury, 1996, and references therein). Moreover, when comparing permeability calculated from the Millington and Quirk (1960) model with that of Moldrup et al. (1996), both agree very well (and for a hydraulic parameter $b = 6$, which corresponds to a typical soil with about 20 % clay, they yield identical values of P; see Fig. S1 in the Supplement). More

ACPD
15, 17397–17448, 2015

importantly, when comparing measured ^{222}Rn profile-based permeability values calculated from Eq. (7a) (see Sect. 3, Table 1) with the model-estimated results, we find the best agreement with these two models (Millington and Quirk, 1960 and Moldrup et al., 1996). The Rogers and Nielson (1991) model seems to overestimate the permeability, particularly during dry conditions, and the Moldrup et al. (1999) model largely underestimates the measured permeability. Therefore, we decided to use the Millington and Quirk (1960) model (Eq. 11), which is solely based on soil porosity and soil moisture, to estimate permeability.

The temperature dependence of the permeability for the ^{222}Rn flux map has been estimated according to Schery and Wasiolek (1998):

$$P(T) = P_0 \left(\frac{T}{273} \right)^{\frac{3}{2}} \quad (12)$$

with T the mean soil temperature in Kelvin and P_0 the permeability at the reference temperature 273 K.

3 Validation of the theoretical concepts to estimate ^{222}Rn fluxes

3.1 Evaluation of measured ^{222}Rn soil profiles and permeability estimates

Schmithüsen (2012) measured the ^{222}Rn exhalation rate and corresponding vertical concentration profiles of ^{222}Rn in a loamy soil close to the Institut für Umweltphysik (IUP) in Heidelberg, Germany. These measurements provide a first validation of the theoretical concept described in Sect. 2, which is used for estimating the ^{222}Rn exhalation rates in Europe from bottom-up data. Measured concentration profiles were binned into mean profiles for dry (θ_w = 0.124, range 0.098–0.145), medium dry (θ_w = 0.199, range 0.160–0.239), and wet (θ_w = 0.311, range 0.264–0.345) soil moisture conditions (Fig. 1). The ranges of the soil moisture classes resulted from a roughly equal distribution of all measured soil moistures (in the upper 20 cm of the soil) during the course of

ACPD
15, 17397–17448, 2015

one year. From fitting a curve according to Eq. (7) to the mean profile data one obtains the parameters $\overline{z}$ and c_∞ as well as values for the ^{222}Rn source strength Q and the permeability P_{exp} (Table 1). The values for Q, which should be the same for all three moisture situations (wet, medium, dry), indeed agree rather well (i.e. to within ± 25 %). The ^{222}Rn exhalation rate at the soil surface ($j_{profile}$) calculated according to Eq. (8) from the parameters fitted to the measured profiles as well as the mean exhalation rates $j_{chamber}$ independently measured using accumulation chambers are also listed in Table 1. They agree within a factor of two for all three soil moisture regimes and within 15 % for the annual mean flux.

For comparison with the measured profile-based permeability, we can calculate the permeability with the Millington and Quirk (1960) model $P_{M\&Q}$ from measured porosity ($\theta_p = 0.368$) and measured mean soil moistures according to Eq. (11). The permeability was adjusted to the mean soil temperatures during the measurement dates for wet, medium and dry conditions according to Eq. (12). Likewise, we use the Rogers and Nielson (1991) model (their Eq. 19) to estimate $P_{R\&N}$. The numbers of $P_{M\&Q}$ and $P_{R\&N}$ are given in the last two columns of Table 1. At our Heidelberg IUP sampling site the Millington and Quirk (1960) model underestimates permeability during wet and dry conditions by up to 25 % while it overestimates permeability during medium dry conditions by about a factor of two. However, the discrepancies between the permeability calculated with the Rogers and Nielson (1991) model and the experimental results are larger at wet and medium dry conditions, while they fit very well at dry conditions ($\theta_w < 0.15$). Using an average $Q = 23.6\,\mathrm{mBq\,m^{-3}\,s^{-1}}$ from the measured profiles and the respective P_i from Table 1, we also estimated Millington and Quirk- and Rogers and Nielson-based soil profiles according to Eqs. (7) and (7a). These profiles are plotted in Fig. 1 for comparison to the observations. Again the Millington and Quirk model fits the observations better than the Rogers and Nielson model. Hence, we favour the Millington and Quirk (1960) model (i.e. Eq. 11) for estimating moisture-dependent permeabilities for all European soils.

ACPD
15, 17397–17448, 2015

3.2 Evaluation of the concept to estimate flux restriction by water table depth

As mentioned in Sect. 2.3, water table depth can be of huge importance limiting the ^{222}Rn exhalation when it rises to levels that are of the same order as $\overline{z}$. These situations are quite frequent in coastal areas, e.g. of Northern Germany or the Netherlands, or in wetland regions. Measurements of co-located ^{222}Rn exhalation rates and shallow water table depths are available from a field site in Federovskoye, Western Russia (Levin et al., 2002). Thus, we can test the validity of Eq. (8a) and compare the solution with the measurements from the Federovskoye transect measurements from Levin et al. (2002, their Fig. 3). The solid lines in Fig. 2 are estimates of the ^{222}Rn exhalation rate for a soil with a mean source strength $Q = 12\,\mathrm{mBq\,m^{-3}\,s^{-1}}$ and relaxation depths $\overline{z}$ of 0.2, 0.35 and 0.5 m (roughly corresponding to wet, medium and dry soil moisture conditions). The parameterization with the water table limitation reproduces the observed relation reasonably well and was thus applied to all areas with shallow water table.

4 Input data for estimation of the ^{222}Rn fluxes from soils in Europe

Estimation of bottom-up ^{222}Rn fluxes for the whole of Europe according to Eq. (8) or Eq. (8a) requires high-resolution data of the following parameters: (1) ^{226}Ra content in the upper soil layers, (2) the distribution of soil types and porosity in the unsaturated soil zone, (3) the emanation coefficient of ^{222}Rn from the soil grains into the soil air, and (4) soil moisture and temperature as well as information on frozen soil. Finally, (5) the water table depth should be known, at least for areas where it is less than 2–3 m below surface. The respective input data used in our high-resolution ^{222}Rn exhalation map are described in the following sections. If available, we compare with independently measured data to have some quantitative evaluation of our input data fields (e.g. for soil moisture).

ACPD
15, 17397–17448, 2015

4.1 ^{226}Ra content in the soil

The ^{226}Ra activity concentration in soils is the governing parameter for the ^{222}Rn flux at the soil surface. It scales linearly with the exhalation rate. The Geochemical Atlas of Europe (Salminen, 2005) summarises results of a European-wide effort within the FOREGS (Forum of European Geological Surveys) Geochemical Baseline Mapping Programme to provide high quality environmental geochemical baseline data for European stream waters, sediments and soils. Besides many other elements and trace constituents, the uranium content was also measured in regularly distributed topsoil and subsoil samples from 26 European countries. Topsoil samples were collected at 0–25 cm depth (with a potential overlying humus layer being removed), while subsoil samples were collected from another 25 cm layer located between 50 and 200 cm depth. Uranium content was measured on residual soil samples (from the < 2 mm grain fraction, with Total Organic Matter (TOC) being removed from these samples) and is reported in mg Uranium per kg residual soil. As total uranium in soil material consists of ca. 99 % of ^{238}U, the values given in the Geochemical Atlas (Salminen, 2005) can be directly transferred into ^{226}Ra activity concentrations, when assuming secular equilibrium between ^{238}U and its daughter ^{226}Ra. The conversion factor from Uranium concentration to ^{238}U activity concentration was taken from IAEA (1989), i.e. 12.35 Bq kg^{-1} per mg kg^{-1} uranium.

The equally distributed 843 individual topsoil uranium measurements (median ± standard deviation: 2.03 ± 2.35 mg kg^{-1}) and the 792 subsoil uranium measurements (median ± standard deviation: 2.00 ± 2.34 mg kg^{-1}) were interpolated by ordinary kriging (e.g. Wackernagel, 2003) for both layers to the 0.083° × 0.083° grid of our map (see Fig. S2 in the Supplement). The resolution of our basic map is restricted in its spatial resolution by that of the global soil texture map of Reynolds et al. (2000), which we used to determine soil texture parameters (see Sect. 4.2). As the uranium content was measured on residual soil samples with total organic carbon being removed, we corrected the activity concentrations for "dilution" with organic carbon, using the

ACPD
15, 17397–17448, 2015

TOC data that have also been reported in the Geochemical Atlas of Europe (Salminen, 2005). This correction is small with typical TOC values in topsoil between 0 and 6 % (median ± standard deviation: 1.73 ± 3.18 %) and in subsoil between 0 and 3 % (median ± standard deviation: 0.40 ± 2.86 %).

For calculating the ^{222}Rn exhalation rates for each pixel, we used the mean values of topsoil and subsoil from the TOC-corrected interpolated ^{226}Ra activity concentrations (i.e. c_{Ra} of Eq. 3). Assuming a depth-constant c_{Ra} seems to be well justified in view of the very good agreement between topsoil and subsoil uranium concentrations reported in the Geochemical Atlas of Europe (Salminen, 2005).

For those regions of our map, for which the uranium content was not available in the Geochemical Atlas (e.g. Belarus, Ukraine), we estimated the ^{226}Ra activity concentration based on geological information available from the high-resolution global lithological map GLiM (Hartmann and Moosdorf, 2012). First, a median ^{226}Ra activity concentration was computed for each lithological class in GLiM using the measured uranium content at all sampling sites together with co-located GLiM data. The resulting relation was then used to extrapolate the ^{226}Ra activity concentration map to the regions not covered by the Geochemical Atlas. Due to this very indirect approach, the resulting ^{222}Rn exhalation rates will have a much higher uncertainty in these regions (hatched area in Fig. S2 in the Supplement).

4.2 Distribution of soil types and estimate of emanation coefficients

Soil texture, i.e. the percentages of sand (0.5–2 mm), silt (0.002–0.5 mm) and clay (< 0.002 mm) for our ^{222}Rn exhalation map have been taken from Reynolds et al. (2000), a soil database that is frequently used in modelling studies of similar problems. Porosity and soil bulk density were computed from soil texture according to Saxton et al. (1986). The data are given at a horizontal resolution of 0.083° × 0.083° and for two different depth intervals (from 0–30 cm and from 30–100 cm). Here we use weighted mean values for 0–100 cm depth for all parameters. As has been shown by Zhuo et al. (2006, 2008), the emanation coefficient ε, i.e. the likelihood of a newly formed ^{222}Rn atom to

ACPD
15, 17397–17448, 2015

escape the grain and reach the air-filled soil volume, depends on the soil type and on soil moisture. The soil moisture dependency is, however, only relevant at very small moisture content below 15 % water saturation (i.e. at $\theta_w < 0.06$ for a typical porosity of $\theta_p = 0.4$). Outside this range ε was shown to be largely constant (Zhuo et al., 2006). For simplicity and because water contents below 15 % saturation are very rare in European soils, we used constant (saturation) values for each texture class. We also neglected the temperature dependence of ε, as it changes by only a few percent within a temperature range of 0–20 °C (Iskandar et al., 2004). The numbers to calculate ε_{sat} for sand, silt and clay are given in Zhuo et al. (2008) in their Table 2. The values must, however, be exchanged, as was noted by Griffith et al. (2010) and confirmed by W. Zhuo (personal communication, 2013). From this we estimated $\varepsilon_{sat} = 0.285$ for sand, $\varepsilon_{sat} = 0.382$ for silt and $\varepsilon_{sat} = 0.455$ for clay. These numbers are well in accordance with emanation coefficients determined by Schüßler (1996) from measured ^{222}Rn profiles and known ^{226}Ra contents in different soils of the surroundings of Heidelberg (M1–M5, see Sect. 5.3 and Table 2). We used weighted mean values for the different texture classes to estimate the emanation coefficients for each pixel of our map.

4.3 Determination of variable soil parameters: soil moisture, temperature, and frost influence

4.3.1 Soil moisture

Soil moisture has a strong impact on the permeability of the soil. Its high temporal and spatial variability makes it a crucial parameter for determining the ^{222}Rn exhalation rate at individual sites. As is illustrated in Fig. 1 and listed in Table 1, the measured mean ^{222}Rn flux from the loamy soil at the IUP sampling site changes by about a factor of six between wet ($\theta_w \approx 0.31$) and dry ($\theta_w \approx 0.12$) conditions. Systematic European-wide soil moisture measurements are still limited. Only few long-term in situ monitoring stations exit. Satellite-derived soil moisture, although providing relatively good spatial coverage, is only representative for the uppermost centimetres of the soil and hence

ACPD
15, 17397–17448, 2015

not suited for our approach. Therefore, we use here soil moisture data simulated by soil models driven by numerical weather prediction models, i.e. these models have been specifically assimilated to determine soil moisture. Two estimates that provide data at high temporal resolution (3 or 6 h) have been used: (1) simulations from the Land Surface Model Noah (driven by NCEP-GDAS meteorological reanalysis), which are part of the Global Land Data Assimilation System GLDAS (Rodell et al., 2004). The spatial resolution of these estimates is $0.25^{\circ} \times 0.25^{\circ}$ with depth intervals of 0–10, 10–40, 40–100 and 100–200 cm; data for the period of 2006–2012 were used. (2) Simulations from the ERA-Interim/Land reanalysis using the latest version of the ECMWF land surface model driven by ERA-Interim atmospheric reanalysis (Balsamo et al., 2015). From this model we used a data set with a horizontal resolution of $0.75^{\circ} \times 0.75^{\circ}$; it has a depth resolution with simulated values for 0–7, 7–28, 28–100 and 100–289 cm and is available until 2010. From both soil moisture models, we calculated vertical means from 0–100 cm depth to cover the same depth interval as the other input parameters. Note that with a relaxation depth of the ^{222}Rn activity concentration profile in the soil of typically 20–100 cm (Table 1), soil parameters of the first 100 cm of the soil are most relevant to describe diffusive transport and the related flux at the soil surface. We further assume here that all parameters do not change with depth and are valid also below 100 cm.

Both soil moisture data sets were compared to observations from the International Soil Moisture Network (ISMN; http://ismn.geo.tuwien.ac.at/; Dorigo et al., 2011). In addition, data from two German sites, Grenzhof near Heidelberg (Wollschläger et al., 2009) and Gebesee, located in North Eastern Germany (O. Kolle, personal communication, 2013), as well as soil moisture data from Binningen, Switzerland (Szegvary et al., 2007b) were used for comparison (see Fig. 7). The performance of the land surface models is summarized in Table S1 in the Supplement. Soil moisture contents of the second and third model layer (10–40 and 40–100 cm for GLDAS-Noah, 7–28 and 28–100 cm for ERA-I/L) were compared to measurements at corresponding depths; mean correlations and mean model-data differences are given for each European network in

ACPD
15, 17397–17448, 2015

ISMN as well as for the additional sites. Both soil moisture estimates correlate well with observations (with a median correlation coefficient of 0.79 for GLDAS-Noah and 0.82 for ERA-I/L), indicating that the temporal variations in monthly mean values are reasonably well captured by the models. On the other hand, substantial differences between modelled and observed mean values exist for some sites and networks (ranging from an underestimation by 60 % to an overestimation by 154 %). This underlines that soil moisture simulated by land surface models is a highly model-specific quantity, which often represents the time variations much better than the absolute magnitude (Koster et al., 2009). For the German sites, as well as for many ISMN sites in Central Europe, the ERA-Interim/Land model estimates higher mean soil moisture for the upper 100 cm than the GLDAS-Noah model. This tendency of ERA-I/L to produce relatively high soil moisture is also confirmed by the study of Balsamo et al. (2015), who found an overestimation of surface soil moisture at the European ISMN sites. Generally, measured soil moisture data fall somewhere in between the two model estimates. Therefore, with all available observations, we cannot per se decide if one or the other model provides more realistic soil moisture estimates.

4.3.2 Spatial resolution and adjustment of soil moisture estimates to grid/pixel porosities

Soil moisture estimates are only available at lower spatial resolution than the other (constant) soil parameters described above. In order to apply internally consistent data sets for the flux estimates, based on the two different soil moisture models, we use the porosities originally applied in the respective land surface model to calculate permeability according to Eq. (11). Consequently, the different flux maps shown in Figs. 3 and 4 have different spatial resolutions. For flux estimates at higher spatial resolution, i.e. $0.083^\circ \times 0.083^\circ$, it will be necessary to make an adjustment of the model estimated soil moisture ($\theta_{w(model)}$) to the porosity of the pixel ($\theta_{p(pixel)}$) to make sure the same free

ACPD
15, 17397–17448, 2015

pore space is available for diffusion according to

$$\theta_{w(pixel)} = \frac{\theta_{w(model)}}{\theta_{p(model)}} \theta_{p(pixel)} \quad (13)$$

In Eq. (13) $\theta_{w(pixel)}$ is the adjusted soil moisture and $\theta_{p(model)}$ is the original porosity used in the soil moisture model. However, in the present paper, we do not show any flux estimates at higher resolution than given by the soil moisture model estimates, but Eq. (13) is used here to adjust modelled soil moisture to the porosities measured at M1–M5 shown in Sect. 5.3 and Fig. 6.

4.3.3 Soil temperature

Soil temperature estimates are available from both soil models that provide soil moisture for the different depths. For respective flux estimates, we thus used these values to calculate the temperature dependence of permeability according to Eq. (12).

4.3.4 Frost

While the reduction of the ^{222}Rn exhalation rate through snow cover is assumed as only minor according to Robertson (2004), the influence of frozen soil on the ^{222}Rn flux may not always be negligible. In order to test its potential impact, we introduced a restriction of the exhalation rate based on atmospheric temperature. A very simple parameterization was used here for comparison with our standard estimates without frost restriction: for each month we have summed up the number of days with maximum air temperature below 0 °C (ice days) and then reduced, for these days, the ^{222}Rn exhalation rate by 50 %. The monthly mean exhalation rate was then calculated as the weighted mean for all days during this month with and without frost. With this parameterization, we implicitly include also some potential effect of snow cover that may be present during ice days. The effect of frost restriction on the flux, compared to our standard estimates where no frost restriction is assumed, is shown in Fig. S3 in the Supplement.

ACPD
15, 17397–17448, 2015

4.4 Water table depth

As in the case of soil moisture, systematic European-wide measurements of water table depth that could be used as input for our ^{222}Rn exhalation map are not existing. Hence, we use data from a hydrological model simulation by Miguez-Macho et al. (2008). Figure S4 shows the distribution of water table depth for Europe, marking large areas of the Netherlands, Northern Italy and Hungary with water table above 2 m. For these areas, the ^{222}Rn exhalation rate was reduced according to our approximation described in Sect. 2.3.

5 Results and discussion

In this section, we first present results for a typical year (2006) of our two ^{222}Rn flux maps, using the two different soil moisture model estimates described in Sect. 4.3.1. Subsequently, we compare the annual mean ^{222}Rn flux of our two European maps for the period 2006–2010 with the earlier published maps of Szegvary et al. (2009) and López-Coto et al. (2013). Before comparing time series of map pixels with observations, the representativeness issue is discussed for the Heidelberg pixel, where Schüßler (1996) performed long-term measurements at locations with different soil types. Finally, we show a comparison of episodic flux measurements with the results of our map and discuss the uncertainties of our approach.

5.1 Distribution of European ^{222}Rn fluxes

Figure 3 shows the maps and frequency distributions of European ^{222}Rn fluxes as estimated with the model parameters described in Sect. 4, applying the two different soil moisture model estimates (GLDAS-Noah (left panels) and ERA-Interim/Land (central panels)) for January (top panels) and July 2006 (middle panels). Both maps show some areas of very high ^{222}Rn exhalations rates, most pronounced in July, which coincide with the areas in Europe where the ^{226}Ra activity concentration in the upper soil

ACPD
15, 17397–17448, 2015

layer is very high. These areas concern for example the Massif Central in Southern France, the Iberian Peninsula and areas in Central Italy (compare ^{226}Ra distribution displayed in Fig. S2 in the Supplement).

For both soil moisture models, we find in many regions seasonal differences of the fluxes that are as large as a factor of two. As mentioned before, these differences originate from the large changes of soil moisture and thus soil permeability between the drier summer and the – in general – wetter winter conditions. The frequency distribution of ^{222}Rn fluxes, displayed in the lower part of Fig. 3, is most confined during winter (January 2006) and when calculated with the ERA-Interim/Land soil moisture data; these fluxes also show a low median value of only 5.81 mBq m^{-2} s^{-1} (IQR = 5.36 mBq m^{-2} s^{-1}). This is about half of the median flux estimated with the GLDAS-Noah soil moisture data set for January 2006 (11.99 mBq m^{-2} s^{-1}). During summer (July 2006), both frequency distributions of fluxes are broader than during winter (IQR: ERA-I/L = 8.49 and GLDAS-Noah = 11.58 mBq m^{-2} s^{-1}). The median values are much larger than in January 2006, i.e. in the case of the ERA-I/L soil moisture more than a factor of two larger, while the difference of the medians in July 2006 between the two maps is much smaller (only about 30 %).

As both maps use the same ^{226}Ra distribution and also the same ^{222}Rn emanation coefficient (i.e. the same ^{222}Rn source term), differences of ^{222}Rn flux of the two maps are solely due to the differences of permeability, which we calculate from modelled soil moisture using the individual soil porosity data from the two models (according to Eq. 11). The right panels in Fig. 3 show the flux differences between the two maps for January and July 2006. In fact, the differences of fluxes between the two maps are not constant all over Europe, but they show a distinct north to south gradient. While fluxes estimated with ERA-I/L soil moisture for January 2006 are slightly higher than those estimated based on GLDAS-Noah in Sweden, Denmark and some parts of Northern Germany and Poland, they are much smaller than GLDAS-Noah-based fluxes in Central and Southern Europe. The differences in soil porosity in the two models are only small (i.e. ERA-I/L uses about 10 % smaller porosity in Northern than in Central Eu-

ACPD
15, 17397–17448, 2015

rope, while porosity is pretty homogeneous all over Europe in GLDAS-Noah and similar to ERA-I/L in Central Europe) but very distinct differences are found in the soil moisture distributions. Soil moisture is much lower in the GLDAS-Noah model estimates for Central and Southern Europe than in ERA-I/L. Only in some areas of Scandinavia and the northern coasts of Central Europe, ERA-I/L estimates lower soil moisture than GLDAS-Noah. This directly translates into higher ^{222}Rn fluxes in the mentioned regions of Scandinavia.

The huge differences between the estimates with different soil moisture input data emphasize the importance of direct comparison of our process-based ^{222}Rn flux estimates with measured fluxes, in order to find out, which soil moisture model would better fit real ambient conditions. This comparison is shown below in Sects. 5.4 and 5.5.

5.2 Comparison of annual mean ^{222}Rn fluxes with those from other published maps

Before comparing with observations at individual sites, we compare the distribution of annual mean fluxes calculated here based on the two soil moisture models for 2006–2010 with the other published European maps of Szegvary et al. (2009) for 2006 and of López-Coto et al. (2013). The latter is shown as climatology for the years 1957–2002. The maps and normalized frequency distributions are displayed in Fig. 4. Zonal averages of 1° latitudinal bands are compared in Fig. 5. The general shape with higher ^{222}Rn exhalation rates in regions of high ^{238}U activity concentrations (e.g., on the Iberian peninsula) is similar in all four maps. The difference between GLDAS-Noah- and ERA-I/L-based fluxes, with generally higher fluxes estimated based on the GLDAS-Noah soil moisture model (except for some areas in Northern Europe), was discussed before for January and July 2006 (Fig. 3) and is also visible in annual mean flux estimates. The annual median values for the 2006–2010 period differ by more than 50 % (Fig. 4, lower four panels). There is relatively good agreement in the spatial pattern, in the annual medians and IQRs between the ERA-I/L and the López-Coto et al. (2013)

ACPD
15, 17397–17448, 2015

map. This is because the basis of the López-Coto et al. (2013) map is also the ^{238}U distribution from the Geochemical Atlas of Europe (Salminen, 2005), and López-Coto et al. (2013) use a similar process-based soil transport model as described here, but the parameterization for permeability developed by Rogers and Nielson (1991). Soil moisture estimates in López-Coto et al. (2013) are from ERA-40 reanalyses, which are based on an earlier version of the land surface model than used in ERA-I/L. Soil moistures in ERA-40 show an overall smaller variability than the ERA-I/L model estimates (Balsamo et al., 2015) used in our study (compare also Sect. 5.4, which discusses time profiles in comparison to observations). The maps of differences between our study and the López-Coto et al. (2013) climatology are displayed in Fig. S5 in the Supplement. While our GLDAS-Noah-based estimates are higher than López-Coto et al. (2013) throughout Europe (with the exception of Northern Ireland and a few areas in Italy) the higher fluxes of our ERA-I/L-based estimates compared to López-Coto et al. (2013) are most prominent in Scandinavia. Differences in annual mean ^{222}Rn fluxes between these two maps are small in Central Europe. The difference in annual fluxes in regions north of 60° N (Fig. 5) might, at least to some extent, be caused by the reduction of ^{222}Rn fluxes in snow-covered regions, which is included in the flux map of López-Coto et al. (2013) but not in our standard estimates. Including a restriction during frozen soil conditions in our flux estimates (orange and cyan lines in Fig. 5) reduces the difference of the annual mean in this region, but they are still more than 50 % higher than López-Coto et al. (2013). However, it is important to keep in mind that López-Coto et al. (2013) use a ca. 40 % smaller emanation coefficient of 0.2 for all soils, compared to a median value of 0.35 in our study. This difference is responsible for a generally 40 % lower ^{222}Rn exhalation rate in the López-Coto et al. (2013) map than estimated for our two maps.

The Szegvary et al. (2009) map has lower spatial resolution and less pronounced hot spots of exhalation rates, but the median of its annual mean exhalation rates lies between our GLDAS-Noah- and ERA-I/L-based estimates. However, as Szegvary et al. (2009) used γ-dose rate observations and an empirical correlation with mea-

ACPD
15, 17397–17448, 2015

sured ^{222}Rn fluxes, their fluxes are significantly different in certain areas of Europe. In particular, the pronounced maximum in the French Massif Central, where high ^{238}U concentrations are measured in the soils (Fig. S2) is only slightly visible in the Szegvary et al. (2009) map. A detailed picture of the differences between our maps and the Szegvary et al. (2009) estimate for 2006 is shown in the Supplement (Fig. S5). Largest differences are seen in Central Europe, where our GLDAS-Noah-based estimates are in many places larger than the Szegvary et al. (2009) estimates by a factor of two, while ERA-I/L-based estimates are often about 50 % smaller compared to the Szegvary et al. (2009) estimates. In Northern Scandinavia our two estimates are higher than the Szegvary et al. (2009) map. The reason might be the shielding effect of snow cover on the observed γ-dose rate (Szegvary et al., 2007a). Including the frost restriction in our flux estimates reduces the difference of the annual mean in this region but leads to values lower than in the Szegvary et al. (2009) map in Southern Scandinavia (Fig. 5).

5.3 Representativeness of local observations to validate the ^{222}Rn flux maps

A large number of systematic direct ^{222}Rn flux measurements using the accumulation chamber technique were carried out in the 1980s and 1990s at five sampling sites south of Heidelberg, Germany. Dörr and Münnich (1990) started these measurements in 1984 at a sandy soil site (M1) as well as in a clay-loam soil site (M4). Schüßler (1996), who sampled additional sites close to the earlier plots from Dörr and Münnich (1990) continued measurements on these plots. The soil parameters of the five sampling sites M1–M5 are listed in Table 2. For these sites we estimated the percentages of clay, silt and sand according to Cosby et al. (1984, Table 2) from the soil type descriptions given by Schüßler (1996). The soil properties of other IUP sampling sites studied by Schell (2004; Gebesee), Schmithüsen (2012; IUP) and Schwingshackl (2013; Gif-sur-Yvette (Gif)) at locations in Germany and France are also listed in Table 2. In addition, the soil parameter values of the $0.083^{\circ} \times 0.083^{\circ}$ pixels from the high-resolution soil parameter

ACPD
15, 17397–17448, 2015

map, in which the measurement sites are located, are listed. From comparison, we can assess the representativeness of the measurement sites for their corresponding pixel of the map. While the Sandhausen sites M1–M3 are not at all representative for the corresponding map pixel, the soil texture and ^{226}Ra activity concentration of the loamy sites M4 and M5 as well as the IUP site, discussed already above (Sect. 3.1), are well comparable with the map pixel. The latter are thus suitable for validation of our maps and the transport model approach. For Gebesee in Northern Germany, actual site parameters agree well with the soil parameters of the map. Only the ^{226}Ra content is about 20 % lower in the map than measured by Schwingshackl (2013). Contrary, for Gif-sur-Yvette in France porosity, bulk density and ^{226}Ra activity concentration are significantly different from the pixel values. This should be kept in mind when comparing our process-based maps with these observations.

Figure 6 shows climatologies of the monthly mean ^{222}Rn exhalation rates measured at the Heidelberg M1–M5 stations over the periods of 1987–1995 (M1, M2, M4) and 1987–1998 (M3, M5). Jutzi (2001) calculated these climatologies from the individual data of regular one- to two-weekly flux measurements reported by Schüßler (1996). The strong dependency of the mean exhalation rate on soil type is clearly visible. The clay or loamy soils (M4 and M5) show the highest fluxes with significant seasonal variations of the exhalation rate with up to a factor of two larger values in July/August compared to January/February. In contrast, the seasonality at M1 and M3 is only very weak and fluxes at the sandy sites (M1–M3) are about three times lower than at M4 and M5.

Figure 6 also shows calculated exhalation rates (according to Eq. 8) based on the measured soil parameters listed in Table 2 and the climatology of soil moisture for the Heidelberg pixel as calculated from the two soil moisture models for the years 2006–2010. Note that for these process-based calculations the GLDAS-Noah used a porosity of $\theta_p = 0.434$ in the map pixels while the ERA-Interim/Land model used $\theta_p = 0.439$, i.e. both significantly different from measured porosities, in particular at the sites with sandy soils (M1 and M3, Table 2). For our calculations, we thus individually adjusted

ACPD
15, 17397–17448, 2015

the soil moistures for all sites M1–M5 according to Eq. (13) to better approximate the pore volumes available for diffusion at the different sites. With these adjustments, the flux estimates based on GLDAS-Noah soil moisture agree very well with observations for the sites M1–M3, but are about 30 % too high for the stations M4 and M5. When using modelled ERA-I/L soil moisture data, estimated mean seasonal ^{222}Rn fluxes are always lower than observations, by up to a factor of three at M1 and M3 and by about a factor of two at the loamy and clay sites M2, M4 and M5. Without adjustment of modelled soil moisture to the site porosities, for all sites and both soil moisture estimates, modelled ^{222}Rn fluxes would be underestimated by up to a factor of six (results not shown in Fig. 6). From this comparison of process-based estimates with long-term observations, we can conclude that (1) the agreement between estimates and observations strongly depends on the validity of soil texture parameters used in the map; (2) modelled soil moisture values need to be adjusted to the local porosity according to Eq. (13), if reliable flux estimates shall be calculated; (3) in the Heidelberg pixels associated to M1–M5, GLDAS-Noah-based ^{222}Rn flux estimates agree rather well to existing observations while ERA-I/L-based estimates largely underestimate fluxes at all sites. This comparison also emphasizes that proper validation of our ^{222}Rn exhalation map is only feasible, if the observations are representative for the pixels of the map. In the case of the sites discussed in Fig. 6, this is true only for sites M4 and M5.

5.4 Comparison of model-based ^{222}Rn flux estimates with measured time series and other flux maps

As demonstrated in the previous section, proper validation of our ^{222}Rn flux estimates requires comparison with direct measurements carried out on soils representative for the respective pixel of the map. However, systematic ^{222}Rn flux measurements in Europe are very sparse so that we include in this section all sites (except for M1–M4 that have already been discussed before, see Sect. 5.3), which have observations available to us over the course of at least four months. Figure 7 compares estimates from our ^{222}Rn flux map based on the two soil moisture models GLDAS-Noah (red lines:

ACPD
15, 17397–17448, 2015

standard, orange: with frost restriction), ERA-I/L (blue lines: standard, cyan: with frost restriction) with those from Szegvary et al. (2009: dark green lines), from López-Coto et al. (2013: light yellow-green lines) and with observations (black dots). Note that in case the observations do not fall into the modelled time span of 2006–2008 displayed here, the data points have been repeated as climatology for all years. If the dotted red and blue lines can be distinguished, they show the effect of shallow water table depth. Fluxes that are not restricted by the water table, contrary to those that are restricted, are then visible as dotted (red and blue) lines (relevant at Lutjewad and Gebesee where the water table is less than 2 m below the soil surface); otherwise, the solid and dotted lines fall onto each other. Figure 7 also shows the soil moisture estimates calculated by the two land surface models as well as direct soil moisture measurements in different depths, if available.

For most sites shown here, the ERA-Interim/Land-based ^{222}Rn fluxes (plotted in blue and cyan) are significantly lower (often by more than a factor of two) than those estimated with the GLDAS-Noah soil moisture data (plotted in red and orange). Accordingly, ERA-I/L soil moisture estimates are significantly higher than those estimated by GLDAS-Noah at these sites; note that porosities do not differ very much in between models at these sites, with a maximum difference of 6 % at Gebesee. Only at Lutjewad the two flux estimates are similar despite the high soil moisture in ERA-I/L; here also the porosity in the ERA-I/L model is by almost a factor of two higher than in GLDAS-Noah. At all sites except for Gif-sur-Yvette and Lutjewad, ERA-I/L-based fluxes are significantly lower than observed fluxes.

At Pallas station in Northern Finland no direct ^{222}Rn flux measurements are available. For this reason, we use flux estimates derived from summer observations in the atmosphere and atmospheric transport modelling (Lallo et al., 2009). For this time of the year, the GLDAS-Noah-based ^{222}Rn flux results compare best with the data. For the winter months, López-Coto et al. (2013) predict very low fluxes at Pallas, and here the effect of frost restriction on GLDAS-Noah- and ERA-I/L-based estimates becomes visible (difference between red and orange resp. blue and cyan lines in Fig. 7a).

ACPD
15, 17397–17448, 2015

A station with very shallow water table is Lutjewad, located at the Netherland's North Sea coast. Not taking into account ground water table restriction in the modelled ^{222}Rn exhalation rate (dotted lines in Fig. 7b) would largely overestimate the flux in both approaches by more than a factor of four. Here the Szegvary et al. (2009) and the López-Coto et al. (2013) models overestimate observed fluxes by more than a factor of two to three. Taking into account the restriction due to the shallow water table brings the modelled ^{222}Rn exhalation rate closer to the observations but also reduces the amplitude of the seasonal variations. Note that ERA-I/L-based and GLDAS-Noah-based fluxes are almost identical under water table restriction and therefore hardly distinguishable in Fig. 7b.

At Gebesee co-located soil moisture measurements are available. They agree very well with the GLDAS-Noah-based model estimates (Fig. 7c) and further, GLDAS-Noah-based ^{222}Rn fluxes fit the observations very well. Here again, the water table depth flux restriction turns out to be important: estimated GLDAS-Noah-based fluxes not restricted by water table depth are significantly higher in early summer than observed fluxes (dotted red line in Fig. 7c), but those restricted by water table agree very well with observations. At the end of the summer, local water table depth may be deeper than in winter and spring, which is why observations then seem to fall on the unrestricted GLDAS-Noah-based model estimates.

As has been indicated already in Fig. 6, the GLDAS-Noah-based estimates for M5-Nußloch are slightly higher than observations while the ERA-I/L-based estimates underestimate the observations by about a factor of two (Fig. 7d). Note, however, that in the current comparison, contrary to the results shown in Fig. 6, we use for both modelled fluxes all parameters, including ^{226}Ra activity concentration and soil porosity from our map and not from observations. Although absolute fluxes are not perfectly reproduced, both our models seem to capture much better the seasonal amplitude of observations than estimates by Szegvary et al. (2009) and López-Coto et al. (2013) models. The good agreement between GLDAS-Noah-based and observed ^{222}Rn fluxes at M5 is accompanied by good agreement of GLDAS-Noah-modelled soil moisture and

ACPD
15, 17397–17448, 2015

respective observations. Soil moisture data plotted for M5 do not exactly stem from the M5 site but are taken from a soil monitoring station north of Heidelberg at Grenzhof (Wollschläger et al., 2009). Modelled soil moistures as well as soil properties in the grid cells corresponding to the location of M5 and Grenzhof are identical in GLDAS-Noah and very similar in ERA-I/l.

At Gif-sur-Yvette, all models except for GLDAS-Noah seem to reproduce well at least the annual mean observed fluxes (Fig. 7e). However, the seasonal amplitude seems to be best captured by the ERA-I/L-based and the GLDAS-Noah-based estimates, whereas the Szegvary et al. (2009) model for 2006, if also valid for other years, and the López-Coto et al. (2013) model underestimate the seasonal amplitude. GLDAS-Noah-based fluxes are larger than observations by about a factor of two. This is very surprising, because ^{226}Ra activity concentration of the map pixel is a factor of two smaller than those measured by Schwingshackl (2013) (see Table 2). From this difference alone, we would expect an underestimation of Gif-sur-Yvette flux observations by both of our flux estimates. On the other hand, the shallow water table at the measurement site (Campoy et al., 2013) might restrict the ^{222}Rn fluxes. This situation is not represented in our maps, where the water table is well below 10 m in this region.

At Binningen, Switzerland, which is the measurement station that Szegvary et al. (2009) also used for the empirical γ-dose rate-based estimates of their ^{222}Rn flux map for 2006, their measured data fall in between our GLDAS-Noah- and ERA-I/L-based fluxes (Fig. 7f). Only in spring 2007 both our estimates are higher than the observed fluxes. Soil moisture estimates in both reanalysis are most of the time lower than the observations but capture the temporal variation rather well. In three summer months of 2006 Szegvary et al. (2009) model estimates are slightly lower than the observations, while the López-Coto et al. (2013) model results are considerably lower than all other model estimates and lower than the observations by at least a factor of two.

In summary, we conclude that at three out of six stations the (generally higher) GLDAS-Noah soil moisture-based ^{222}Rn exhalation rates are in good agreement with

ACPD
15, 17397–17448, 2015

observations. At two of these sites, where we have data available, this correlates with good agreement of model-calculated and observed soil moisture. Flux estimates based on ERA-Interim/Land soil moistures have the tendency to underestimate observed fluxes and only fit well at one of our comparison sites (Gif-sur-Yvette). The two published maps, in particular that developed by López-Coto et al. (2013), generally underestimate measured fluxes with the exception of the coastal site Lutjewad. There the shallow water table depth is not taken into account in these models, which leads to large over-estimation. Concerning the seasonal amplitude of fluxes, the GLDAS-Noah-based estimates as well as those based on ERA-I/L soil moisture are in most cases very well in line with observations. Contrary, Szegvary et al. (2009) flux estimates largely underestimate seasonal amplitudes, at least in 2006. The same is true for the López-Coto et al. (2013) model estimates. As mentioned before, a large part of the general underestimation by López-Coto et al. (2013) may be due to the use of a too low emanation coefficient in their estimates. Based on available observations, the effect of frozen soils cannot be evaluated. However, restriction due to shallow water table turns out to be important, not only at the coastal site Lutjewad, but potentially also in river plains such as in the surroundings of the Gebesee site.

5.5 Comparison with published episodic ^{222}Rn flux observations

Since only very few systematic ^{222}Rn flux measurements during different seasons are available in the literature, validation of our new ^{222}Rn flux map is far from exhaustive. In order to better judge at least the reliability of the European-wide flux estimates, we have compiled here all published ^{222}Rn flux measurements available to us, even if they are only based on episodic field campaigns (see Table S2 in the Supplement). Larger short-term data sets from a single site have been averaged to monthly values. Figure 8 (left panel) shows the geographical distribution of these episodic observations and their individual values colour-coded. The frequency distribution of these measured ^{222}Rn fluxes are shown in Fig. 8 (right part, black histogram) in comparison to the frequency distributions of the respective monthly mean values estimated for

ACPD
15, 17397–17448, 2015

the corresponding pixels of the flux maps based on the two soil moisture data sets (red histogram: GLDAS-Noah, blue histogram: ERA-I/L). While the observations yield a median value of 12.22 mBq m^{-2} s^{-1} (IQR = 13.49 mBq m^{-2} s^{-1}), the GLDAS-Noah-based model gives a median of 15.03 Bq m^{-2} s^{-1} (IQR = 9.47 mBq m^{-2} s^{-1}) and the ERA-I/L-based estimates a median of 7.43 Bq m^{-2} s^{-1} (IQR = 5.61 mBq m^{-2} s^{-1}). The median of observations is about 40 % higher than the ERA-I/L-based flux estimates while it is about 20 % lower than the GLDAS-Noah-based estimates. This is in accordance with the earlier comparison based on more systematic long-term results at fewer stations, discussed in Sect. 5.4,

5.6 Discussion of uncertainties

5.6.1 Soil moisture

Temporal and spatial variations of soil moisture have a huge influence on the permeability in the soil and thus on the ^{222}Rn exhalation rate. This can clearly be seen when comparing the GLDAS-Noah-based and the ERA-I/L based ^{222}Rn flux maps. Using our observations at the Heidelberg IUP site we find that the permeability differences during dry and wet conditions are as large as a factor of 20, leading to differences in the fluxes up to a factor of seven (Table 1). When comparing model estimated soil moisture values with respective observations it is not clear, if one or the other soil moisture model would generally provide more realistic values (see Table S1 in the Supplement). Likewise, comparison of ^{222}Rn flux map results with observations does not allow favouring one or the other soil moisture model. While annual mean fluxes may be over- or underestimated by one of the models, both capture the seasonal amplitude of the fluxes very well. The same is true for the seasonal amplitudes of the soil moisture estimated by both models. This indicates that there may be some systematic shortcomings in the parameterization of the soil moisture models or a conceptual difference in the meaning of the variable “soil moisture” in the models (Koster et al., 2009). In cases where the soil moisture at a station is correctly captured by one of the models, we also find good

ACPD
15, 17397–17448, 2015

agreement between the ^{222}Rn flux estimated by that model and the measured one (e.g. GLDAS-Noah at Gebesee and M5/Grenzhof).

5.6.2 Permeability model

Even if we had good estimates of soil moisture, we need to keep in mind that the Millington-Quirk (1960) model used in this study does not necessarily describe permeability in the unsaturated soil zone correctly. Comparison of model-based permeability with permeability estimated from observed ^{222}Rn soil profiles (Fig. 1) shows differences as large as a factor of two at medium dry conditions. This may translate into differences of the fluxes of similar size during these conditions. Therefore, also shortcomings in the parameterization of permeability may considerably contribute to the uncertainty of the ^{222}Rn flux. However, using different parameterizations as e.g. the one of Rogers and Nielson (1991), as done by Griffiths et al. (2010) and López-Coto et al. (2013) does not improve the situation (see Table 1).

5.6.3 ^{226}Ra content

An important parameter determining the ^{222}Rn flux from the soil is the ^{226}Ra content. Here we have used an interpolated ^{238}U distribution based on systematic measurements published in the European Geochemical Atlas (Salminen, 2005). Uncertainties in the soil sample analysis (Sandström et al., 2005) and the interpolation are both less than 10 %. From the interpolated ^{238}U distribution, we estimated ^{226}Ra activity concentration by assuming secular equilibrium between ^{238}U and its daughter ^{226}Ra. This assumption may not always be fulfilled at all sites due to preferential leaching of ^{234}U from the soil grains, so that our ^{238}U-based equilibrium estimate of ^{226}Ra must be seen as an upper limit of the true ^{226}Ra values. However, when comparing the ^{226}Ra values from the map with point measurements made at IUP Heidelberg, we find satisfactory agreement if other soil parameters, such as texture and bulk density, are similar, i.e. if the point measurement is representative for the pixel (data not shown). An example

ACPD
15, 17397–17448, 2015

of obvious differences between the soil characteristics of our measurement site and the pixel of the map is Gif-sur-Yvette, France. Here we observe a factor of two higher ^{226}Ra activity concentration in our measurement than assumed for the map pixel, but also bulk density and porosity show a large difference.

5.6.4 Emanation coefficient

Besides the ^{226}Ra activity concentration in the bulk soil material, the emanation coefficient is an essential parameter for correctly estimating the ^{222}Rn exhalation rate. Only few measurements of the emanation coefficients for different soil types and environmental conditions exist and reported values span a wide range of 0.05 to 0.7 (Nazaroff, 1992). The emanation coefficient estimates of our study compare well with the observation-based estimates by Schüßler (1996) around the Heidelberg site. The averaged value used in our study (0.35) is by 75 % higher than the constant emanation coefficient of 0.2 used by López-Coto et al. (2013) for all soils. The underestimation of the ^{222}Rn fluxes by the López-Coto et al. (2013) model at most sites indicates that an emanation coefficient of 0.2 is probably too small. More measurements of emanation coefficients and their dependence on soil texture would be helpful to reduce the uncertainty in this parameter.

5.6.5 Constancy of transport parameters with depth

One basic assumption in our estimate is homogeneity of soil parameters with depth up to 1 m. While the differences of ^{238}U in the European Geochemical Atlas between upper and lower soil layers are only minor, other soil parameters such as porosity and texture may not be as homogeneous with depth. Porosity derived from the Reynolds et al. (2000) soil texture data set differs by ca. 3 % between the two soil layers, but this presumably underestimates vertical variability. The largest vertical inhomogeneity is most probably that of soil moisture. During summer months, at one of our sampling sites we observed that soil moisture differs by a factor of two between 30 and

ACPD
15, 17397–17448, 2015

90 cm depths (see Fig. 7 for M5 Nußloch). However, the differences between the two soil models, GLDAS-Noah and ERA-I/L can be even larger. Therefore, with the current reliability of soil moisture input data from the models, our simplification assuming homogeneous parameters throughout the unsaturated soil seems justified. In any case, except for dry summer conditions, more than three quarters of the total ^{222}Rn flux at the soil surface originate from the upper 50 cm of the soil; one should thus make sure that all parameters in this upper layer are determined as reliable as possible.

5.6.6 Soil texture

For consistency, we use in our European ^{222}Rn flux estimations the same porosity as applied in the soil moisture simulations of the respective land surface model. In both models, the soil properties were derived from the FAO Digital Soil Map of the World (FAO DSMW), however from different versions (Reynolds et al., 2000; FAO, 2003), and indeed soil porosities in both models are very similar. Only parts of Northern Europe show differences of up to 10 %. Soil databases are constantly improving as more soil information is collected and more detailed digital soil data sets are becoming available, like the Harmonized World Soil Database (HWSD, FAO/IIASA/ISRIC/ISSCAS/JRC, 2012) and the Global Soil Data set for use in Earth System Models (GSDE; Shangguan et al., 2014), which should reduce uncertainties associated with soil texture. However, the comparisons between soil properties in these new data sets (in Shangguan et al., 2014) also reveal maximum porosity differences of around 10 % in Northern Europe.

5.6.7 Frost

In our sensitivity test with a very simple parameterization of frost and/or snow conditions, ^{222}Rn flux estimates in Scandinavia and Eastern Europe are reduced by 30–40 % during winter and by 10 % for annual mean fluxes in this region. However, due to the lack of systematic flux measurements during winter conditions, this parameterization could not be evaluated and can only give an estimate of the associated uncertainties.

ACPD
15, 17397–17448, 2015

For more reliable estimations of ^{222}Rn fluxes in higher latitudes during winter, more investigations on the influence of frost and snow on ^{222}Rn exhalation is desirable.

6 Conclusions and perspectives

A high-resolution ^{222}Rn flux map for Europe was developed based on a parameterization of ^{222}Rn production and transport in the soil. The approach includes a well-established parameterization of soil permeability (Millington and Quirk, 1960) and makes use of existing data sets of soil properties, uranium content, model-derived soil moisture as well as model-derived water table depth. Comparisons with direct ^{222}Rn flux measurements in different regions of Europe indicate that the observed seasonality is realistically reproduced by our approach, which was not achieved by earlier studies, and confirms the validity of estimating permeability in soil air based on the Millington and Quirk (1960) model.

However, using two different sets of soil moisture reanalyses also reveals the strong dependence of the reliability of our ^{222}Rn flux estimates on realistic soil moisture values. While both model-based soil moisture estimates evaluated here seem to reproduce realistically the observed seasonality in soil moisture, which translates into a realistic seasonality of ^{222}Rn exhalation rates in both realizations of our flux map, the overall magnitude of the ^{222}Rn fluxes differs. Soil moisture estimates could largely be improved with better soil models. Currently available models show large deviations in their estimates; however, comparison with observations from the soil moisture network does not allow any univocal ranking.

The spatial resolution of the soil moisture models used here restricts spatial resolution of the two realizations of our European ^{222}Rn exhalation map. In many applications, such as the Radon-Tracer-Method (e.g. Levin et al., 1999), local estimates of ^{222}Rn fluxes are required. In such cases, our theoretical approach could easily be applied using measured soil moisture data, which become more and more available at ecosystem sites in Europe or elsewhere (e.g. FLUXNET, Baldocchi et al., 2001). In our

ACPD
15, 17397–17448, 2015

study, we restricted the temporal resolution to one month because (quasi-) continuous ^{222}Rn flux measurements are not available for comparison. However, extension of the temporal resolution to that of the soil moisture models is easily achievable.

Validation of our estimated ^{222}Rn fluxes was restricted in our study to only few observational sites, most of them located in Central Europe. Many climate zones and soil types such as subarctic regions, wetlands and dry areas of Europe, could not be validated with observations. This includes quantification of the influence of snow cover or frozen soils. Hence, additional systematic ^{222}Rn flux measurements would facilitate a further validation of the presented maps.

It would be extremely helpful to apply our approach to other areas of the world. However, this is hampered by the un-availability of a systematic ^{238}U or ^{226}Ra survey in other regions and continents. Empirical correlations between ^{226}Ra activity concentrations and other soil parameters turned out to be only weak and do not allow for accurate evaluations of the ^{222}Rn source over large regions.

The presented ^{222}Rn flux maps for Europe are directly available for atmospheric transport studies. As we cannot unambiguously identify which of the soil moisture reanalysis is more reliable, we propose to use an "ensemble mean" of the two maps, thereby reducing the potential systematic effect introduced by the soil models. Furthermore, in cases when soil moisture is directly available in the transport model (as in most online transport models) our approach could also be applied using the model-generated soil moisture.

Digital versions of the maps are available from the authors upon request.

The Supplement related to this article is available online at doi:10.5194/acpd-15-17397-2015-supplement.

Acknowledgements. The research leading to these results has received funding from the European Community's Seventh Framework Programme (FP7/2007-2013) in the InGOS project under grant agreement no 284274. We thank G. Miguez-Macho (Universidade de Santiago de

ACPD
15, 17397–17448, 2015

Compostela, Spain) for providing the model-simulated water table depth data set, N. Manohar (Center for Isotope Research, University of Groningen, the Netherlands) for making available the ^{222}Rn flux measurements in Lutjewad, and Felix Vogel (Laboratoire des Sciences de Climat et de l'Environnement, Gif-sur-Yvette, France) for helping with the flux measurement in Gif-sur-Yvette. We further thank O. Kolle (Max-Planck-Institute for Biogeochemistry, Jena, Germany) for providing soil moisture measurements in Gebesee and A. Gassama (Institut für Umweltphysik, Universität Heidelberg, Germany) for providing soil moisture measurements in Grenzhof. The GLDAS-Noah soil moisture data used in this study were acquired as part of the mission of NASA's Earth Science Division and archived and distributed by the Goddard Earth Sciences (GES) Data and Information Services Center (DISC). ERA-Interim/Land soil moisture reanalysis data were obtained from the ECMWF Data Server.

The article processing charges for this open-access publication were covered by the Max Planck Society.

References

Baldocchi, D., Falge, E., Gu, L., Olson, R., Hollinger, D., Running, S., Anthoni, P., Bernhofer, C., Davis, K., and Evans, R.: FLUXNET: a new tool to study the temporal and spatial variability of ecosystem-scale carbon dioxide, water vapor, and energy flux densities, B. Am. Meteorol. Soc., 82, 2415–2434, 2001.

Balsamo, G., Albergel, C., Beljaars, A., Boussetta, S., Brun, E., Cloke, H., Dee, D., Dutra, E., Muñoz-Sabater, J., Pappenberger, F., de Rosnay, P., Stockdale, T., and Vitart, F.: ERA-Interim/Land: a global land surface reanalysis data set, Hydrol. Earth Syst. Sci., 19, 389–407, doi:10.5194/hess-19-389-2015, 2015.

Born, M., Dörr, H., and Levin, I.: Methane consumption in aerated soils of the temperate zone, Tellus B, 42, 2–8, 1990.

Chevillard, A., Ciais, P., Karstens, U., Heimann, M., Schmidt, M., Levin, I., Jacob, D., and Podzun, R.: Transport of ^{222}Rn using the on-line regional scale model REMO: a detailed comparison with measurements over Europe, Tellus B, 54, 850–871, 2002.

Campoy, A., Ducharne, A., Cheruy, F., Hourdin, F., Polcher, J., and Dupont, J. C.: Response of land surface fluxes and precipitation to different soil bottom hydrological conditions in a gen-

ACPD
15, 17397–17448, 2015

eral circulation model, J. Geophys. Res.-Atmos., 118, 10725–10739, doi:10.1002/jgrd.50627, 2013.
Conen, F. and Robertson, L.: Latitudinal distribution of radon-222 flux from continents, Tellus B, 54, 127–133, 2002.
Cosby, B. J., Hornberger, G. M., Clapp, B., and Ginn, T. R.: A statistical exploration of the relationships of soil moisture characteristics to the physical properties of soils, Water Resour. Res., 20, 682–690, 1984.
Dorigo, W. A., Wagner, W., Hohensinn, R., Hahn, S., Paulik, C., Xaver, A., Gruber, A., Drusch, M., Mecklenburg, S., van Oevelen, P., Robock, A., and Jackson, T.: The International Soil Moisture Network: a data hosting facility for global in situ soil moisture measurements, Hydrol. Earth Syst. Sci., 15, 1675–1698, doi:10.5194/hess-15-1675-2011, 2011.
Dörr, H. and Münnich, K. O.: ^{222}Rn flux and soil air concentration profiles in West Germany. Soil ^{222}Rn as tracer for gas transport in the unsaturated soil zone, Tellus B, 42, 20–28, 1990.
FAO: Digital Soil Map of the World and Derived Soil Properties, Food and Agriculture Organization of the United Nations, Land and Water Digital Media Series, CD-ROM, Rome, Italy, 2003.
FAO/IIASA/ISRIC/ISSCAS/JRC: Harmonized World Soil Database (version 1.2), FAO, Rome, Italy, IIASA, Laxenburg, Austria, 2012.
Griffiths, A. D., Zahorowski, W., Element, A., and Werczynski, S.: A map of radon flux at the Australian land surface, Atmos. Chem. Phys., 10, 8969–8982, doi:10.5194/acp-10-8969-2010, 2010.
Hartmann, J. and Moosdorf, N.: The new global lithological map database GLiM: a representation of rock properties at the Earth surface, Geochem. Geophy. Geosy., 13, Q12004, doi:10.1029/2012GC004370, 2012.
Hirao, S., Yamazawa, H., and Moriizumi, J.: Estimation of the global ^{222}Rn flux density from the Earth's surface, Jpn. J. Health Phys., 45, 161–171, 2010.
IAEA: Construction and Use of Calibration Facilities for Radiometric Field Equipment, International Atomic Energy Agency, Vienna, Austria, Technical Reports Series 309, 86 pp., 1989.
Iskandar, D., Yamazawa, H,., and Iida, T.: Quantification of the dependency of radon emanation power on soil temperature, Appl. Radiat. Isotopes, 60, 971–973, 2004.
Jacob, D. J. and Prather, M. J.: Radon-222 as a test of convective transport in a general circulation model, Tellus B, 42, 118–134, 1990.

ACPD
15, 17397–17448, 2015

Jin, Y. and Jury, W. A.: Characterizing the dependence of gas diffusion coefficient on soil properties, Soil Sci. Soc. Am. J., 60, 66–71, 1996.
Jutzi, S.: Verteilung der Boden-Radon Exhalation in Europa, Staatsexamensarbeit, Institut für Umweltphysik, Heidelberg University, Germany, 57 pp., 2001.
Koster, R. D., Guo, Z., Yang, R., Dirmeyer, P. A., Mitchell, K., and Puma, M. J.: On the nature of soil moisture in land surface models, J. Climate, 22, 4322–4335, doi:10.1175/2009JCLI2832.1, 2009.
Lallo, M., Aalto, T., Hatakka, J., and Laurila, T.: Hydrogen soil deposition in the northern boreal zone, Boreal Environ. Res., 14, 784–793, 2009.
Levin, I., Glatzel Mattheier, H., Marik, T., Cuntz, M., Schmidt, M., and Worthy, D. E.: Verification of German methane emission inventories and their recent changes based on atmospheric observations, J. Geophys. Res., 104, 3447–3456, 1999.
Levin, I., Born, M., Cuntz, M., Langendörfer, U., Mantsch, S., Naegler, T., Schmidt, M., Varlagin, A., Verclas, S., and Wagenbach, D.: Observations of atmospheric variability and soil exhalation rate of Radon-222 at a Russian forest site: technical approach and deployment for boundary layer studies, Tellus B, 54, 462–475, 2002.
López-Coto, J., Mas, J. L., and. Bolivar, J. P.: A 40-year retrospective European radon flux inventory including climatological variability, Atmos. Environ., 73, 22–33, doi:10.1016/j.atmosenv.2013.02.043, 2011.
Manohar, S. N., Meijer, H. A. J., Neubert, R. E. M., Kettner, E., and Herber, M. A.: Radon flux measurements at atmospheric station Lutjewad – analysis of temporal trends and main drivers controlling the emissions, submitted, 2015.
Miguez-Macho, G., Li, H., and Fan, Y.: Simulated water table and soil moisture climatology over North America, B. Am. Meteorol. Soc., 89, 663–672, doi:10.1175/BAMS-89-5-663, 2008.
Millington, R. J. and Quirk, J. P.: Transport in porous media, in: Proceedings of the 7th International Congress of Soil Science, 14–24 August 1960, Madison, Wisconsin, USA, 97–106, 1960.
Millington, R. J. and Quirk, J. P.: Permeability of porous solids, T. Faraday Soc., 57, 1200–1207, 1961.
Moldrup, P., Kruse, C. W., Rolston, D. E., and Yamaguchi, T.: Modeling diffusion and reaction in soils: II I. Predicting gas diffusivity from the Campbell soil-water retention model, Soil Sci., 161, 366–375, 1996.

ACPD
15, 17397–17448, 2015

Moldrup, P., Olesen, T., Yamaguchi, T., Schjönning, P., and Rolston, D. E.: Modeling diffusion and reaction in soils: IX. The Buckingham–Burdine–Campbell Equation for gas diffusivity in undisturbed soil, Soil Sci., 164, 542–551, 1999.

Nazaroff, W.: Radon transport from soil to air, Rev. Geophys., 30, 137–160, 1992.

Rasch, P. J., Feichter, J., Law, K., Mahowald, N. Benkovitz, C., Genthon, C., Giannakopoulos, C., Kasibhatla, P., Koch, D., Levy, H., Maki, T., Prather, M., Roberts, D. L., Roelofs, G.-J., Stevenson, D., Stockwell, Z., Taguchi, S., Kritz, M., Chipperfield, M., Baldocchi, D., McMurray, P., Barrie, L., Balkanski, Y., Chatfield, R., Kjellstrom, E., Lawrence, M., Lee, H. N., Lelieveld, J., Noone, K. J., Seinfeld, J., Stenchikov, G., Schwartz, S., Walcek, C., and Williamson, D.: A comparison of scavenging and deposition processes in global models: results from the WCRP Cambridge Workshop of 1995, Tellus B, 52, 1025–1056, 2000.

Reynolds, C., Jackson, T., and Rawls, W.: Estimating soil water-holding capacities by linking the Food and Agriculture Organization soil map of the world with global pedon databases and continuous pedotransfer functions, Water Resour. Res., 36, 3653–3662, 2000.

Robertson, L. B.: Radon emissions to the atmosphere and their use as atmospheric tracers, PhD thesis, University of Edinburgh, United Kingdom, 237 pp., 2004.

Rodell, M., Houser, P. R., Jambor, U., Gottschalck, J., Mitchell, K., Meng, C.-J., Arsenault, K., Cosgrove, B., Radakovich, J., Bosilovich, M., Entin, J. K., Walker, J. P., Lohmann, D., and Toll, D.: The Global Land Data Assimilation System, B. Am. Meteorol. Soc., 85, 381–394, doi:10.1175/BAMS-85-3-381, 2004.

Rogers, V. C. and Nielson, K. K.: Correlations for predicting air permeabilities and ^{222}Rn diffusion coefficients of soils, Health Phys., 61, 225–230, 1991.

Salminen, R. (Ed.): Geochemical Atlas of Europe. Part 1: Background Information, Methodology and Maps, Geological Survey of Finland, Espoo, Finland, 2005.

Sandström, H., Reeder, S., Bartha, A., Birke, M., Berge, F., Davidsen, B., Grimstvedt, A., Hagel-Brunnström, M.-L., Kantor, W., Kallio, E., Klaver, G., Lucivjansky, P., Mackovych, D., Mjartanova, H., van Os, B., Paslawski, P., Popiolek, E., Siewers, U., Varga-Barna, Z., van Vilsteren, E., and Ødegård, M.: Sample preparation and analysis, in: Geochemical Atlas of Europe, Part 1: Background Information, Methodology and Maps, edited by: Salminen, R., Geological Survey of Finland, Espoo, Finland, 81–94, 2005.

Saxton, K., Rawls, W. J., Romberger, J., and Papendick, R.: Estimating generalized soil-water characteristics from texture, Soil Sci. Soc. Am. J., 50, 1031–1036, 1986.

ACPD
15, 17397–17448, 2015

Schell, S.: ^{222}Radon-Profil-Messungen in Süd- und Ostdeutschland, Anwendung der Radon-Tracer-Methode zur Berechnung von CO_2- und CH_4-Flüssen, Diplomarbeit, Institut für Umweltphysik, Heidelberg University, Germany, 106 pp., 2004.

Schery, S. D. and Wasiolek, M. A.: Modeling radon flux from the Earth's surface, in: Radon and Thoron in the Human Environment, World Scientific Publishing, Singapore, 207–217, 1998.

Schmithüsen, D.: Atmospheric and soil flux radon measurements in Heidelberg, Diplomarbeit, Institut für Umweltphysik, Heidelberg University, Germany, 66 pp., 2012.

Schüßler, W.: Effektive Parameter zur Bestimmung des Gasaustauschs zwischen Boden und Atmosphäre, PhD thesis, Heidelberg University, Germany, 1996.

Schwingshackl, C.: Experimental Validation of a Radon-222 Flux Map, Master Thesis, Institut für Umweltphysik, Heidelberg University, Germany, 100 pp., 2013.

Shangguan, W., Dai, Y., Duan, Q., Liu, B., and Yuan, H.: A global soil data set for earth system modeling, J. Adv. Model. Earth Syst., 6, 249–263, doi:10.1002/2013MS000293, 2014.

Sun, K., Guo, Q., and Zhuo, W.: Feasibility for Mapping Radon Exhalation Rate from Soil in China, J. Nucl. Sci. Technol., 41, 86–90, 2004.

Szegvary, T., Conen, F., Stöhlker, U., Dubois, G., Bossew, P., and de Vries, G.: Mapping terrestrial γ-dose rate in Europe based on routine monitoring data, Radiat. Meas., 42, 1561–1572, doi:10.1016/j.radmeas.2007.09.002, 2007a.

Szegvary, T., Leuenberger, M. C., and Conen, F.: Predicting terrestrial ^{222}Rn flux using gamma dose rate as a proxy, Atmos. Chem. Phys., 7, 2789–2795, doi:10.5194/acp-7-2789-2007, 2007b.

Szegvary, T., Conen, F., and Ciais, P.: European ^{222}Rn inventory for applied atmospheric studies, Atmos. Environ., 43, 1536–1539, doi:10.1016/j.atmosenv.2008.11.025, 2009.

Taguchi, S., Law, R. M., Rödenbeck, C., Patra, P. K., Maksyutov, S., Zahorowski, W., Sartorius, H., and Levin, I.: TransCom continuous experiment: comparison of ^{222}Rn transport at hourly time scales at three stations in Germany, Atmos. Chem. Phys., 11, 10071–10084, doi:10.5194/acp-11-10071-2011, 2011.

Turekian, K. K., Nozaki, Y., and Benninger, L. K.: Geochemistry of atmospheric radon and radon products, Annu. Rev. Earth Pl. Sc., 5, 227–255, 1977.

Wackernagel, H.: Multivariate Geostatistics: an Introduction with Applications, Springer, Berlin, 2003.

Wilkening, M. H., Clements, W. E., and Stanley, D.: Radon-222 flux measurements in widely separated regions, in: The Natural Radiation Environment, edited by: Adams, J. A. S., Low-

ACPD
15, 17397–17448, 2015

der, W. M., and Gesell, T. F., 11, USAEC Report CONF-720805-P2, National Technical Information Service, Springfield, VA, 717 pp., 1972.
Wollschläger, U., Pfaff, T., and Roth, K.: Field-scale apparent hydraulic parameterisation obtained from TDR time series and inverse modelling, Hydrol. Earth Syst. Sci., 13, 1953–1966, doi:10.5194/hess-13-1953-2009, 2009.
Zhuo, W., Iida, T., and Furukawa, M.: Modeling radon flux density from the Earth's surface, J. Nucl. Sci. Technol., 43, 479–482, 2006.
Zhuo, W., Guo, O., Chen, B., and Cheng, G.: Estimating the amount and distribution of radon flux density from the soil surface in China, J. Environ. Radioactiv., 99, 1143–1148, 2008.

ACPD
15, 17397–17448, 2015

Table 1. Parameters of the fit curves plotted in Fig. 1, mean exhalation rates estimated from the measured radon concentration profiles ($j_{profile}$) and directly measured with flux chambers ($j_{chambers}$) at the same site as well as mean permeability as estimated from the experimental data (P_{exp}), from the Millington and Quirk (1960) model ($P_{M\&Q}$) and from the Rogers and Nielson (1991) model ($P_{R\&N}$).

Profile	c_∞ Bq m^{-3}	Q mBq m^{-3} s^{-1}	$\overline{z}$ m	$j_{profile}$ mBq m^{-2} s^{-1}	$j_{chamber}$ mBq m^{-2} s^{-1}	θ_w	P_{exp} m^2 s^{-1}	$P_{M\&Q}$ m^2 s^{-1}	$P_{R\&N}$ m^2 s^{-1}
wet	10 000	21.0	0.20	4.3	6.8	0.311	0.86×10^{-7}	0.72×10^{-7}	0.52×10^{-7}
medium	9900	20.8	0.38	7.8	13.5	0.199	2.97×10^{-7}	6.59×10^{-7}	10.3×10^{-7}
dry	13 800	29.0	0.97	28	14.7	0.124	19.6×10^{-7}	14.2×10^{-7}	20.9×10^{-7}

ACPD
15, 17397–17448, 2015

Table 2. Characteristics of the long-term ^{222}Rn flux sampling sites from IUP (compare Fig. 1 and Table 1), M1–M5 close to Heidelberg as well as Gebesee, Northern Germany, and Gif-sur-Yvette, France. For M1–M5 the percentage of clay, silt and sand have been estimated from the soil type description of Schüßler (1996), according to mean percentages reported by Cosby et al. (1984, Table 2); the ^{226}Ra activity concentrations have been reported by Schüßler (1996). For IUP, Gebesee and Gif-sur-Yvette, these parameters were measured by Schwingshackl (2013). For comparison with measurements, we also list the data for the respective pixels from the high-resolution map of soil parameters ("pixel") (ε: emanation coefficient, θ_p: soil porosity, ρ_b: dry bulk density).

Site	Location	Measurement Period	Clay %	Silt %	Sand %	ε	θ_p	ρ_b kg m^{-3}	^{226}Ra Bq kg^{-1}
M1: Sandhausen	49.35° N, 8.65° E	1987–1995	6	12	82	0.307	0.365	1540	9.4
M2: Sandhausen	49.35° N, 8.65° E	1987–1995	10	32	58	0.333	0.430	1510	14
M3: Sandhausen	49.35° N, 8.65° E	1987–1998	6	12	82	0.307	0.350	1630	8.4
M1–M3 pixel	49.38° N, 8.63° E	2006–2010	15	22	63	0.332	0.436	1495	37
M4: Nußloch	49.3° N, 8.72° E	1987–1995	27	15	58	0.346	0.425	1540	34
M5: Nußloch	49.3° N, 8.72° E	1987–1998	27	15	58	0.346	0.425	1540	38
M4, M5 pixel	49.29° N, 8.71° E	2006–2010	15	22	63	0.332	0.436	1495	38
IUP: Heidelberg	49.42° N, 8.68° E	2011–2012	19	37	44	0.353	0.368	1440	36
IUP pixel	49.46° N, 8.71° E	2006–2010	15	22	63	0.332	0.436	1495	37
Gebesee	51.10° N, 10.92° E	2003–2004	36	62	2	0.406	0.480	1370	38
Gebesee pixel	51.13° N, 10.96° E	2006–2010	28	39	34	0.369	0.491	1349	31
Gif	48.72° N, 2.17° E	2013	16	79	5	0.390	0.370	1650	40
Gif pixel	48.71° N, 2.13° E	2006–2010	28	39	33	0.371	0.493	1345	18

ACPD
15, 17397–17448, 2015

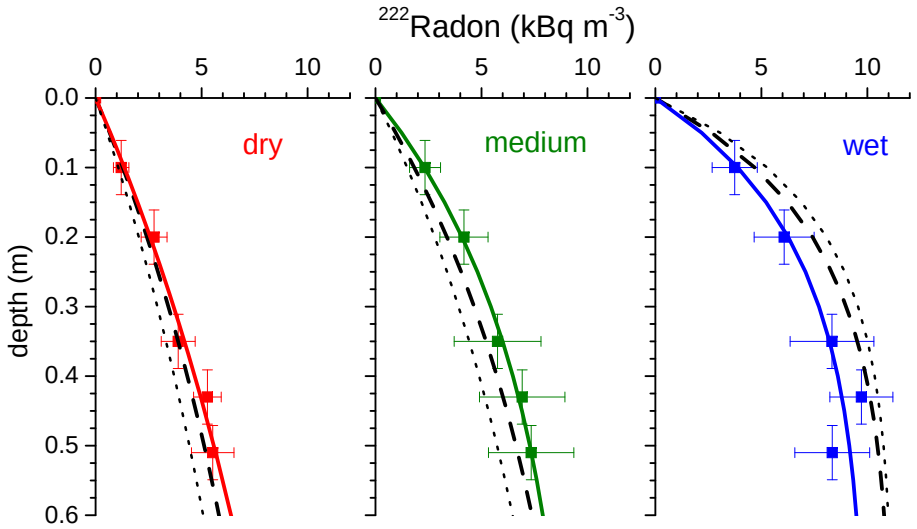

Figure 1. Mean vertical profiles of the ^{222}Rn activity concentrations measured in a soil in Heidelberg (IUP) averaged over dry (mean $\theta_w = 0.124$), medium dry (mean $\theta_w = 0.199$) and wet (mean $\theta_w = 0.311$) soil moisture conditions in 2011–2012. The coloured lines are fitted curves through the data according to Eq. (7). The dashed lines are activity concentration profiles calculated with permeability estimated with the Millington and Quirk (1960) model, while dotted lines are respective profiles calculated with the permeability model from Rogers and Nielson (1991). Both estimates use the measured soil porosity ($\theta_p = 0.368$), mean θ_w and soil temperature during the measurements as well as a mean source strength $Q = 23.6\,\mathrm{mBq\,m^{-3}\,s^{-1}}$, i.e. the mean from all measured profiles estimated according to Eq. (7a) (i.e. mean of Table 1, third column).

ACPD
15, 17397–17448, 2015

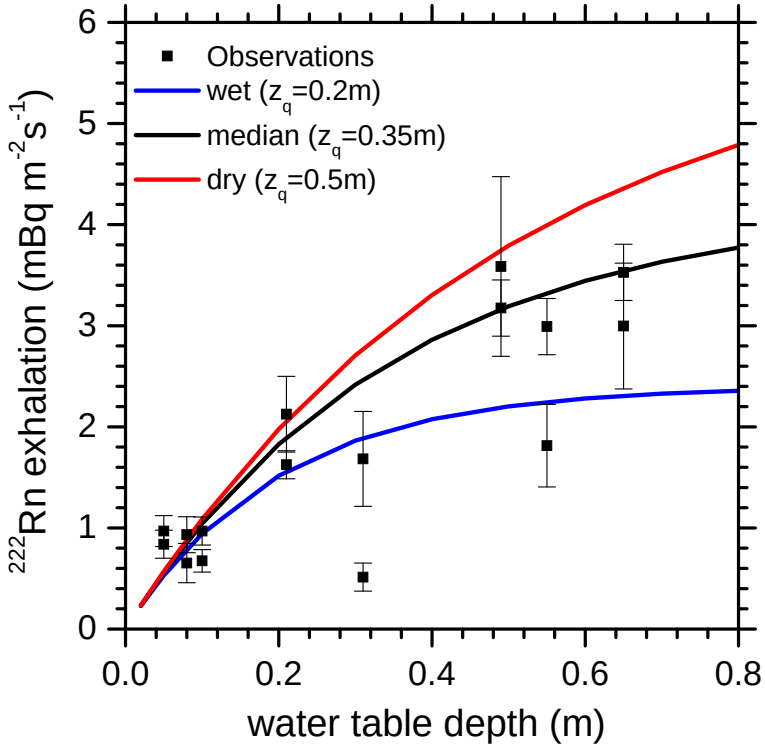

Figure 2. Dependency of the ^{222}Rn exhalation rate on water table depth; the solid lines are calculated according to Eq. (8a) with $Q = 12\,\mathrm{mBq\,m^{-3}\,s^{-1}}$ and different permeabilities resp. relaxation depths $\overline{z}\,(= z_q)$.

ACPD
15, 17397–17448, 2015

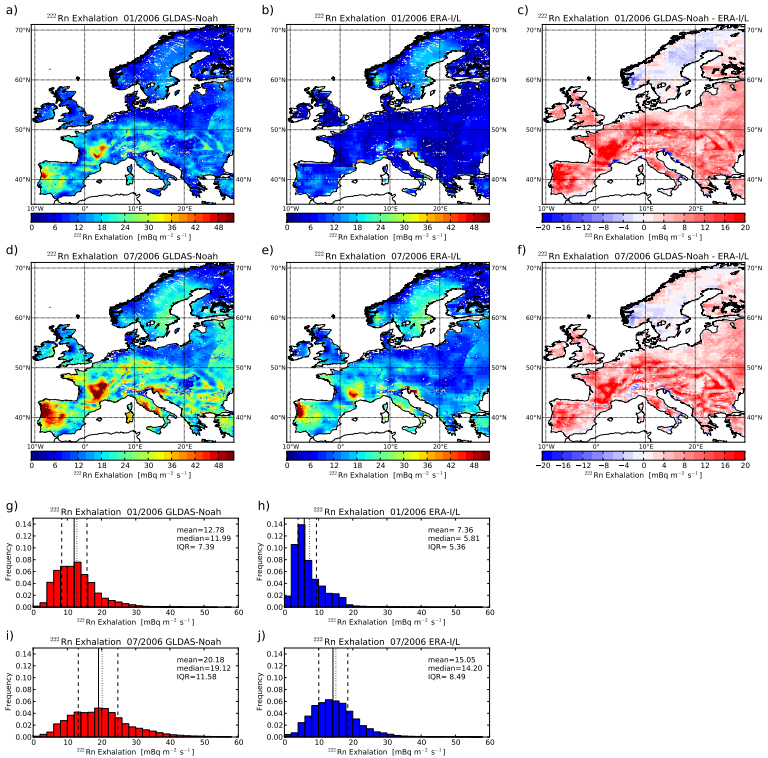

Figure 3. ^{222}Rn exhalation rate maps of European soils, their differences and frequency distributions for January and July 2006. The left panels show the flux maps and normalized frequency distributions calculated with the monthly mean soil moisture estimates from the GLDAS-Noah LSM for January and July 2006, while the middle panels show respective estimates with the ERA-Interim/Land model. The mean values, median values and the Inter Quartile Range (IQR) of the normalized frequency distributions of January and July 2006 fluxes (in $\mathrm{mBq\,m^{-2}\,s^{-1}}$) are also given. The right panels show the differences between GLDAS-Noah- and ERA-Interim/Land-based fluxes.

ACPD
15, 17397–17448, 2015

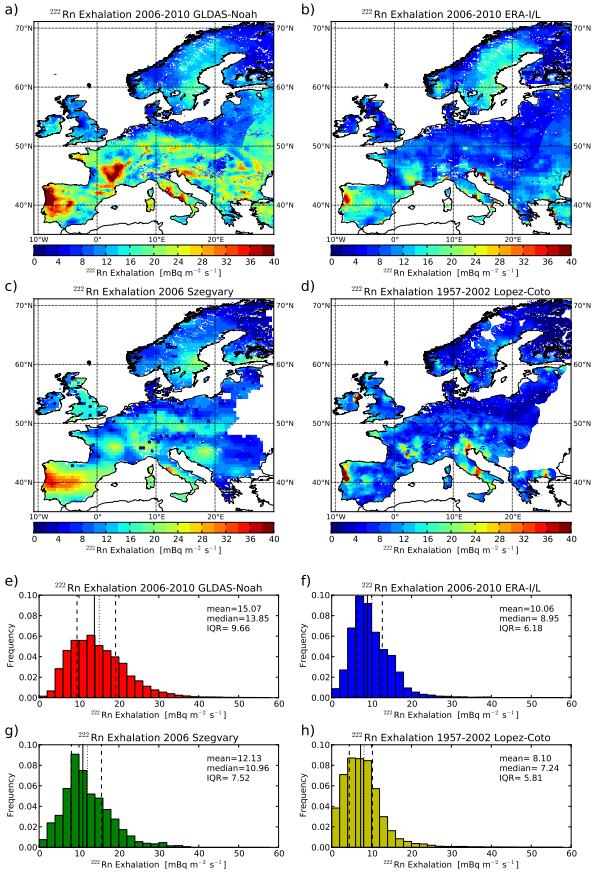

Figure 4. Annual mean ^{222}Rn exhalation rates for 2006–2010 from this study in comparison with published maps (Szegvary et al., 2009; Lopez-Coto et al., 2013). The upper four panels show the geographical distributions, while the lower four panels display the normalised frequency distributions of annual means from all pixels of the four maps.

ACPD
15, 17397–17448, 2015

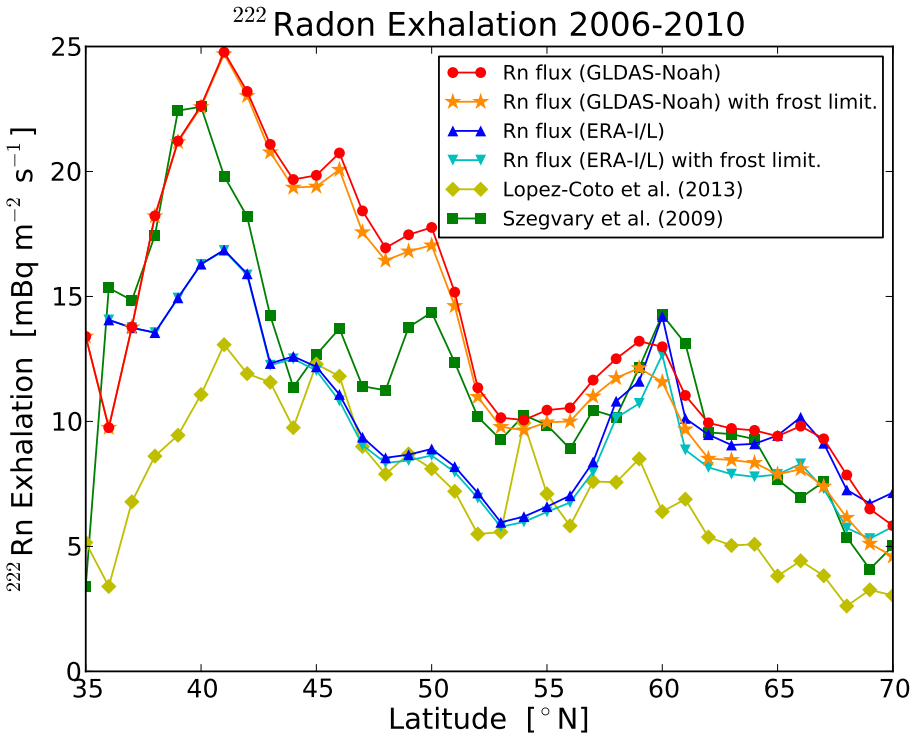

Figure 5. Latitudinal gradient of annual mean ^{222}Rn exhalation rates for 2006–2010 from this study in comparison with published maps (Szegvary et al., 2009; Lopez-Coto et al., 2013). Zonal average land surface fluxes for 1° latitude bands are shown.

ACPD
15, 17397–17448, 2015

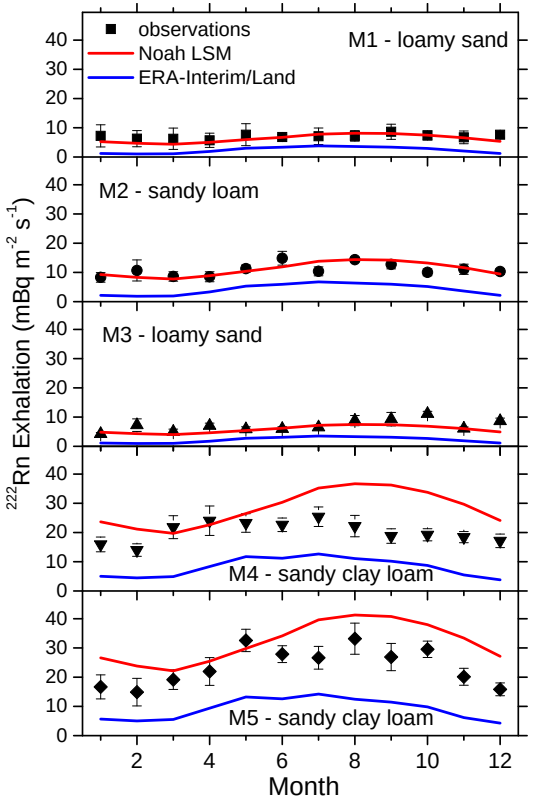

Figure 6. Comparison of the observed climatology of monthly ^{222}Rn fluxes at the sampling sites M1–M5 (symbols with error bars representing monthly mean observational data and their standard error) with bottom-up estimates using the permeability estimate of Millington and Quirk (1960). Soil moisture climatology is taken either from the GLDAS-Noah LSM (red lines) or from the ERA-Interim/Land model (blue lines) for the respective pixels, averaged over the period of 2006–2010. Note that the monthly soil moisture values have been adjusted according to Eq. (13), i.e. taking into account the actual porosity at the measurement sites (see text).

ACPD
15, 17397–17448, 2015

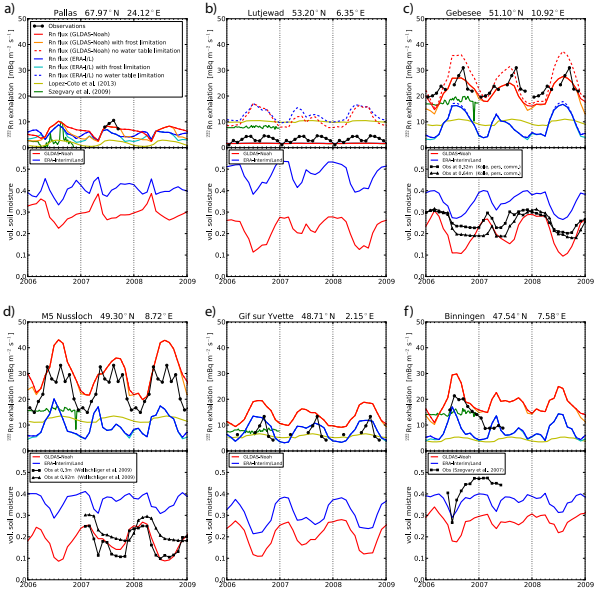

Figure 7. Upper panels of each row: comparison of model estimated ^{222}Rn fluxes (coloured lines) with monthly mean observations (solid black dots) at selected European sites. The flux data have been taken from the following publications: Pallas 2007 data: Lallo et al. (2009); Lutjewad multi-year mean data: Manohar et al. (2015); Gebesee 2003–2004 data: Schell (2004); M5 Nußloch 1985–1997 climatology: Jutzi (2001); Gif-sur-Yvette 2013 data: Schwingshackl (2013); Binningen 2006–2007 data: Szegvary et al. (2007b, http://radon.unibas.ch). Also included in the upper graphs of both rows are flux estimates from Szegvary et al. (2009) for the year 2006 and from López-Coto et al. (2013) for the years 1957–2002 plotted as seasonal cycle climatology. Lower panels of each row: Comparison of GLDAS-Noah (red lines) and ERA-I/L (blue lines) estimated monthly mean soil moisture with observations. The soil moisture data were taken from the following publications: Gebesee: data from O. Kolle (personal communication, 2013); M5 Nußloch: Grenzhof data from Wollschläger et al. (2009); Binningen: Szegvary et al. (2007b, http://radon.unibas.ch).

ACPD
15, 17397–17448, 2015

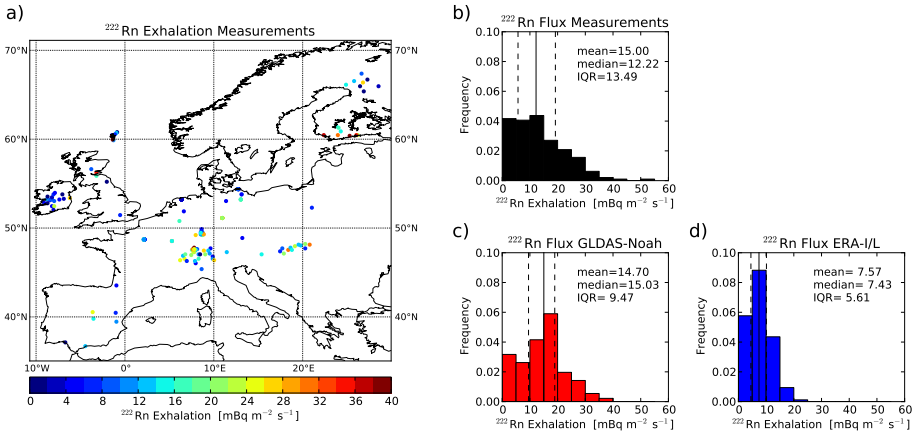

Figure 8. Map of episodic ^{222}Rn flux observations in Europe (left panel) and their frequency distribution (black histogram) in comparison to those of monthly values of the corresponding pixels of our two ^{222}Rn maps (GLDAS-Noah: red histogram, ERA-I/L: blue histogram). All measurement data are provided in the Supplement (Table S2).

ACPD
15, 17397–17448, 2015

A process-based ^{222}Rn flux map for Europe

U. Karstens et al.